NASA TECHNICAL NOTE

NASA TN D-6101

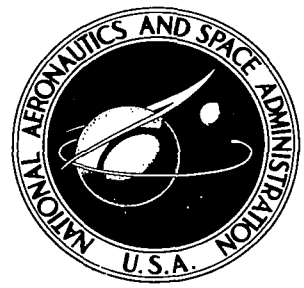

NASA TN D-6101
c.1

NASA TN D-6101

EXPLORATORY INVESTIGATION OF THE STRUCTURE OF THE TIP VORTEX OF A SEMISPAN WING FOR SEVERAL WING-TIP MODIFICATIONS

by James Scheiman and James P. Shivers

Langley Research Center
Hampton, Va. 23365

NATIONAL AERONAUTICS AND SPACE ADMINISTRATION • WASHINGTON, D. C. • FEBRUARY 1971

1. Report No.	2. Government Accession No.	3. Recipient's Catalog No.
NASA TN D-6101		

4. Title and Subtitle	5. Report Date
EXPLORATORY INVESTIGATION OF THE STRUCTURE OF THE TIP VORTEX OF A SEMISPAN WING FOR SEVERAL WING-TIP MODIFICATIONS	February 1971
	6. Performing Organization Code

7. Author(s)	8. Performing Organization Report No.
James Scheiman and James P. Shivers	L-7309
	10. Work Unit No.
9. Performing Organization Name and Address	721-01-10-02
NASA Langley Research Center Hampton, Va. 23365	11. Contract or Grant No.
	13. Type of Report and Period Covered
12. Sponsoring Agency Name and Address	Technical Note
National Aeronautics and Space Administration Washington, D.C. 20546	14. Sponsoring Agency Code

15. Supplementary Notes

16. Abstract

Wind-tunnel tests were performed on a semispan wing with rather radical wing-tip modifications. These modifications were chosen in an attempt to deform, displace, or modify the cross-sectional characteristics of the trailing tip vortex.

The wing-tip modifications tested did not grossly affect the spanwise lift distribution and did not produce a noticeable change in the position of the downstream tip vortex. Tip-vortex cross-sectional variations were obtained such that the outer flow field was no longer potential flow.

17. Key Words (Suggested by Author(s))	18. Distribution Statement
Tip vortex Vortex core size Wind-tunnel tests Vortex structure Wing-tip effect	Unclassified – Unlimited

19. Security Classif. (of this report)	20. Security Classif. (of this page)	21. No. of Pages	22. Price*
Unclassified	Unclassified	45	$3.00

*For sale by the National Technical Information Service, Springfield, Virginia 22151

EXPLORATORY INVESTIGATION OF THE STRUCTURE OF THE TIP VORTEX OF A SEMISPAN WING FOR SEVERAL WING-TIP MODIFICATIONS

By James Scheiman and James P. Shivers
Langley Research Center

SUMMARY

Wind-tunnel tests were performed on a semispan wing with rather radical wing-tip modifications. These modifications consisted of a leading-edge disk flow spoiler, a trailing-edge disk flow spoiler, a porous wing-span extension, and a tip adjustable air jet-sheet ejector. These modifications were chosen in an attempt to deform, displace, or modify the cross-sectional characteristics of the trailing tip vortex. The tests were performed at a Reynolds number of 2.64×10^6 and data were obtained up to 9 chord lengths behind the wing.

The wing-tip modifications tested did not grossly affect the spanwise lift distribution and did not produce a noticeable change in the position of the downstream tip vortex. Tip-vortex cross-sectional variations were obtained with the wing-tip modifications. These cross-sectional variations indicate an increase in the turbulence in the flow-field area outside the core such that this area was no longer potential flow. It is believed that this additional turbulence outside the core area is caused by axial velocity variations along the vortex radius. The blowing tip jet did not have any noticeable effect on the tip-vortex cross-sectional characteristics.

The experimental results indicate that the core diameter increases in proportion to the square root of the downstream distance. Further, the core diameter increases in direct proportion to the lift coefficient.

INTRODUCTION

A fundamental understanding of the structure of the rotor-blade tip vortex and a means of controlling it are of particular importance with regard to rotor noise and dynamic loads. A review of the literature indicates that there is a lack of basic information on the tip vortex of fixed wings and very little fundamental information on the tip vortex of rotor blades. This lack of fundamental knowledge has retarded the development of engineering solutions to numerous helicopter problems. For example, reference 1

presents information relative to the difficulties encountered in predicting the trajectory of the tip vortex for the hovering helicopter and its effect on hovering performance. Reference 2 gives results of attempts to improve overall rotor performance by delaying compressibility effects by modifying the blade tip. Reference 3 discusses the phenomenon of discrete noise that is generated by a rotor blade intersecting the tip vortex shed by a preceding blade in the rotor system.

In an effort to gain some engineering control of the tip vortex, a wind-tunnel investigation has been conducted to investigate the changes in the tip-vortex characteristics of a fixed wing when the tip configuration is changed. The tip vortex of a fixed wing does not, of course, accurately represent the vortex of a rotor blade. It was believed, however, that fixed-wing tests would show up significant variations in the tip vortex. In the present investigation, a semispan wing model with various tip shapes was tested in the Langley full-scale tunnel over a range of angles of attack from -4° to 24°. The tunnel speed was about 140 feet per second (42.7 meters per second) which represents a Reynolds number of about 2.6×10^6.

SYMBOLS

C_D wing drag coefficient, $\frac{D}{\frac{1}{2}\rho V_\infty{}^2 S}$

C_L wing lift coefficient, $\frac{L}{\frac{1}{2}\rho V_\infty{}^2 S}$

C_μ jet coefficient, $\frac{m_j V_j}{\frac{1}{2}\rho V_\infty{}^2 c^2}$

c wing chord, feet (meters)

D aerodynamic drag, pounds (newtons)

L aerodynamic lift, pounds (newtons)

m_j jet mass-flow rate, slugs per second (kilograms per second)

r radial distance from vortex center, feet (meters)

S	wing reference area, feet^2 (meter^2)
V_j	jet velocity, feet per second (meters per second)
V_t	tangential velocity about vortex core, feet per second (meters per second)
V_∞	free-stream wind velocity, feet per second (meters per second)
x,y,z	downstream coordinates of center of vortex, see figure 9
α	wing angle of attack, degrees
ρ	mass density of air, slugs per foot^3 (kilograms per meter^3)

APPARATUS AND TESTS

This test program was conducted in the 30- by 60-ft (9 by 18 m) Langley full-scale tunnel. The semispan wing was installed on the tunnel scale system with its span axis vertical and the root end mounted flush with the ground board in the center of the turntable. The wing angle-of-attack variations were made by rotating the turntable through selected angles. The model aerodynamic forces were measured and recorded on the tunnel magnetic tape system.

Model

Photographs of the basic semispan wing tip and the wing-tip modifications are shown in figure 1. The basic semispan wing, configuration 1, had a squared-off tip (fig. 1(a)). The airfoil coordinates and physical properties are given in table I. This configuration was included to provide a basis for evaluation of the effects of the more unconventional wing-tip modifications.

Model configuration 2 consisted of the basic model with a thin circular $5\frac{1}{2}$-in.-diameter (14 cm) disk fixed to the leading edge of the airfoil (fig. 1(b)) such that its axis was alined with the chord line. Model configuration 3, shown in figure 1(c), is the same as configuration 2 except that the disk was mounted at the airfoil trailing edge rather than at the leading edge. The intent of configurations 2 and 3 was to produce a periodic ring vortex in a plane perpendicular to the axis of the tip vortex and thus affect the sheet vortex rollup process and also the final tip-vortex core size. Configuration 2, with the disk at the leading edge, would be expected to strongly influence lift distribution near the wing tip, whereas configuration 3 would be expected to have a much lesser lifting effect; but since the rolling up process has been demonstrated to start near the leading edge of

the wing tip (ref. 2), configuration 3 might be expected to strongly influence the immediate rollup process.

Model configuration 4 (fig. 1(d)) was achieved by adding a porous plate to the wing tip and alining it along the wing chord. This plate added 6 in. (15.2 cm) to the wing span and was 24 in. (61 cm) long in the chord direction. References 4 and 5 indicate that by adding a porous wing tip to a full-scale aircraft a significant increase in core size and decrease in tangential velocity were achieved immediately behind the wing; however, far downstream the velocity was reduced only slightly. Configuration 4 was included to explore and to verify these results.

Model configuration 5, shown in figure 1(e), was obtained by removing the squared-off wing tip cap (configuration 1) and exposing a cylinder with a longitudinal slot through which compressed air could be exhausted in a jet sheet. The cylinder axis was alined along the wing chord. The physical properties of this configuration are given in table II. The cylinder could be rotated about its own axis such that the jet sheet of air could be directed in any direction between $\pm 90^{\circ}$ from the span axis of the semispan wing, 0° being in the spanwise direction in which the jet sheet was effectively an extension of the wing span. The air supplied to the jet could be throttled to obtain various jet velocities. The purpose for testing configuration 5 was to verify and expand the results of reference 6 which indicated that by tip blowing, the tip-vortex core displacement downstream could be changed. Thus, it may be possible to control this displacement by controlling the tip jet blowing rate. Configuration 5 (jet blowing) tests were made at three blowing angles, 0°, 45°, and 90°. The angles are measured from the wing span axis, positive being the case in which the rotated jet sheet extends in a negative lift direction (jet blowing in the direction of downwash). Two mass-flow rates were chosen for each jet blowing angle. (See table III.)

Tuft Grid and Photographic System

A 3- by $4\frac{1}{2}$-ft (0.91 by 1.37 m) tuft grid was mounted on the survey carriage in the full-scale wind tunnel to survey the tip vortex. The individual tufts were mounted on a 1-in. (2.54 cm) grid spacing. A sequence camera, for permanent recording of the tuft grid and a television camera, for observation, were mounted at the entrance to the exit cone. The television camera gave continuous monitoring capability and a direct instantaneous view of the results seen by the still camera. Photographs were taken at each model test angle of attack at specific downstream tuft-grid locations.

Photographs of the tuft grid were taken with the grid 1, 3, 5, 7, and 9 chord lengths downstream from the trailing edge of the semispan wing. Two photographs were taken at each position and whenever the vortex motion was unsteady additional photographs were taken. This unsteadiness was not anticipated and it was hoped that the additional

photographs would provide statistical time average data. The vortex core positions were read on each photograph within an estimated accuracy of ±1 in. (±2.54 cm). Nonrepeatability of the vortex position with time (i.e., fixed-tuft grid) could thus be attributed to either reading error (within ±1 in.) or vortex core movement or a combination of both. The displacement of the vortex core in a plane perpendicular to the free-stream velocity was referenced to the semispan wing tip and the quarter-chord axis.

Test Program

The test program consisted of photographing the tuft grid and measuring the semispan wing forces simultaneously for various angles of attack and with the tuft grid located at various distances downstream of the wing. With the exception of part of the testing of configuration 1, the test program was all run at approximately the same tunnel speed, 140 ft/sec (42.7 m/sec). This tunnel speed resulted in a Reynolds number of approximately 2.6×10^6. The model angle-of-attack variations were from -4^o to 24^o.

The semispan wing forces were measured with the existing external balance system. Fifty force data points were taken automatically for each test point in order to obtain good average data.

RESULTS AND DISCUSSION

The discussion is presented in three sections: Force Data, Tip-Vortex Position, and Tip-Vortex Cross Section. For constant-chord wing, which has a nonelliptic lift distribution, the strongest trailing vortices will exist near the wing tip. It is these same trailing tip vortices that will roll up first and are closest to the vortex core. Therefore, wing-tip modifications might be expected to effect a change in the tip vortex and, thus, to have a large effect on the downstream vortex cross-sectional characteristics. A tuft grid was photographed at preselected chord lengths downstream of the wing tip to determine the downstream vortex characteristics. Actually, it was possible in these tests to investigate the tip vortex only about one-half as far downstream of the tip as would be the location of the following blade of a helicopter, 9 chords as compared with about 20 chords. It is believed, however, that the measurements were made far enough downstream to determine whether there were any significant effects. The lift and drag forces on the wing were also measured to afford an aerodynamic definition of the test conditions and to determine the effects of the tip configurations on lift and drag.

Force Data

Figures 2 to 5 present the lift and drag coefficients for configurations 1 to 4, respectively. The data for the basic wing without any modifications (configuration 1)

are superimposed on figures 3, 4, and 5 for comparison. Figures 3 and 4 indicate an increase in drag and a loss in lift as would be expected with the disk mounted normal to the airstream at the tip. The data also show that, with the disk at the leading edge of the airfoil (configuration 2, fig. 3), the lift loss is greater than that when the disk is located at the trailing edge (configuration 3, fig. 4).

In figure 5 for configuration 4, there is an increase in the lift-curve slope over that for the basic wing (configuration 1). This result is probably due to the effective increase in wing area and/or in the aspect ratio. This result is consistent with some results of the wind-tunnel tests of reference 7. In addition, the results herein and the results of reference 7 indicate an unacceptable increase in drag.

The basic force data for configuration 5 with no blowing is shown in figure 6. These data are also superimposed on the force data for blowing (figs. 7 and 8).

Figure 7(a), for blowing in a spanwise direction, indicates no discernible difference between partial blowing and no blowing; whereas figure 7(b), for full blowing, indicates an increase in lift and an increase in drag. This result disagrees with the results of reference 6 which indicate an increase in lift and a decrease in drag. However, the results of reference 6 were obtained with jet velocities up to 10 times the free-stream velocity whereas the jet velocity for figure 7(b) was only about 5 times free-stream velocity. The increase in lift can be associated with an effective increase in aspect ratio caused by spanwise blowing. Figure 8, for moderate blowing $\left(C_{\mu} = 0.00741\right)$ downward 45° from the spanwise direction, does not indicate any significant difference between blowing and no blowing. Unfortunately, an unaccountable zero shift in the force data occurred which invalidated the force data for full blowing at 45° and blowing at 90°.

Tip-Vortex Position

The tip-vortex position is defined by three coordinates shown in figure 9. The x position is downstream from the semispan wing trailing edge with the wing at 0° angle of attack and is given in terms of chord lengths. The z position is measured from the quarter-chord axis and is positive in the negative lift direction (positive downwash). The y vortex position is measured in the direction of the wing span axis from the wing tip surface along the quarter-chord axis and is positive toward the wing root.

The tip-vortex motion for four angles of attack for configurations 1 and 5 are shown in figures 10 and 11, respectively. Since the tip-vortex location was not steady, figures 10 and 11 have been prepared to show the degree of movement involved. Also shown in figure 10 is the theoretical displacement from equation (28) of reference 8. These figures show test points representing the location of the center of the vortex as determined from several photographs taken for the same nominal condition but at different times. In

general, the results indicate that the displacement y/c and z/c of the center of the vortex increases with increasing angle of attack (i.e., increasing lift or increasing circulation) which agrees with theory (ref. 8). It can be seen that the lateral variation z/c (unsteadiness) in the vortex motion at a given x/c position is in many cases as large as the total average displacement. Note also that the magnitude of the variation increases as the downstream position x/c increases. Experimental results of numerous investigators indicate that the vortex position is steady. (For example, see refs. 6, 8, and 9.) Hence it must be assumed that the unsteadiness of the vortex in the present tests was the result of gustiness of the tunnel airstream.

If it is assumed that a gust persists for at least the time required for the fluid to move 9 chord lengths, approximately 0.2 sec, then a tip vortex would be displaced downstream within a cone and the magnitude of the displacement would increase as the downstream distance increases. If all measured variations are attributed to such gustiness, the flow angularity variations appear to be approximately $\pm 0.5^{\circ}$. This degree of gustiness is consistent with dynamic measurements of the stream angularity in the proximity of the tip vortex.

The effect of the geometric changes to the tip on the tip-vortex position is shown in figure 12 which compares the tip-vortex displacement for configurations 1 to 4 for angles of attack of 16° and 18°. The lift coefficient for each configuration is tabulated since the wing tip shape could change C_L even though α was constant (the bound circulation is proportional to lift or C_L and not α). If the same tunnel gustiness is assumed to occur for all models and the limited number of photographs is assumed to represent good statistical averages, it can be concluded that none of these configurations had any noticeable effect on downstream tip-vortex displacement.

The effect of spanwise blowing at the tip is shown in figure 13 for angles of attack of 16° and 18°. It appears that there is no noticeable difference for the three blowing rates including no blowing. This result does not agree with the results in reference 6. However, the tip jet velocities herein are lower than in reference 6. The maximum mass-flow rate used in the present tests, however, was chosen as being representative of the maximum value that could be achieved with bleed air from the engines of current helicopters; therefore, it could be concluded that spanwise blowing from the blade tip of a helicopter would not have any significant effect on the tip-vortex displacement for practical levels of blowing.

Figures 14 and 15 present the tip-vortex displacement comparison for various blowing rates for a downward blowing jet at 45° and 90°, respectively, from the wing span axis. The results are for wing angles of attack of 16° and 18°. Again there is no significant effect of the jet blowing on the position of the tip vortex.

In summary of the survey of the tip-vortex position, within the limits of variations due to gustiness and resolution, it may be stated that none of the wing-tip modifications tested, which were very gross modifications, caused any significant change in the downstream position of the tip vortex.

Tip-Vortex Cross Section

Besides the position characteristics of the vortex, the cross-sectional characteristics (perpendicular to the core axis) can be evaluated. The vortex core characteristics are of particular importance. The vortex core is defined herein as the area inside the circle whose radius is defined as the radius at which the tangential fluid velocity is a maximum. The area outside the core is generally accepted as being potential flow and the area inside the core can have axial and radial velocity components. The core fluid is rotational (nonpotential flow) and the theory is much more complex. Having the capability of increasing the core size will result in a decrease in the maximum induced velocities within the vortex. For the tests herein the vortex appeared to be completely rolled up at the 1-chord position; therefore, no evaluation was made of the rolling-up process.

Figures 16 and 17 present vortex core size information. Reference 8 indicates that for a uniform downwash (elliptical spanwise loading) the theoretical rolled-up core size is directly proportional to the wing span. Applying this theory to configuration 1 results in a constant core-diameter—wing-chord ratio of approximately 0.28. Reference 4 indicates that the measured velocity is much less than the theoretical; therefore, the actual core size would correspondingly be expected to be much larger than this theoretical value of 0.28. The measurements herein verify this conclusion. Figure 16 is a plot of the approximate core size with downstream position for configuration 1 at an angle of attack of 16°. The figure shows that the core size increases slightly in proportion to the downstream position. The results of references 4 and 9 indicate that the core size varies as $A + B\sqrt{x/c}$ and $B\sqrt{x/c}$, respectively, where A and B are constants. These functions are plotted in figure 16 where the constant coefficients in the functions are chosen by a least-square fit. As seen from the figure, the data appear to agree with the theory.

Figure 17 is the approximate core size plotted against lift coefficient and angle of attack for configuration 1 at a constant 5 chord lengths downstream. The core size increases directly with increasing lift coefficient. This trend is in agreement with the results of reference 4 which indicate that the boundary layer shed from the trailing edge ultimately rolls up into the core (the boundary-layer thickness being proportional to the lift).

Figure 18 is a plot of the nondimensional tangential velocity against the radial distance from the center of the vortex for configuration 1 at $\alpha = 8^{\circ}$ and $x/c = 5$. The nondimensional tangential velocities were determined by assuming that each tuft alined

itself along the maximum velocity vector, that the tufts are the same length (2.5 in. (6.35 cm)), and that the tuft grid does not interfere with the flow field. By appropriate trigonometric manipulations, the measured velocities were determined. The theoretical velocity distribution from reference 9, namely,

$$V_t = \frac{1.4V_{t,max}r_{core}}{r}\left[1 - e^{-1.2\left(\frac{r}{r_{core}}\right)^2}\right]$$

is also shown in figure 18. The unknown constants r_{core} (vortex core radius) and $V_{t,max}$ (maximum tangential core velocity) were determined by a least-square fit calculation. The correlation indicates that the experimentally measured tangential velocity distribution agrees well with the theory.

Figures 19 to 23 present photographs of the cross section of various tip vortices. Since duplicate photographs were taken at each test condition in an attempt to obtain some statistical data, these figures have identical titles and the test conditions differ only by a time factor (about a second or two). Although some of these figures are for different chord length positions (x/c coordinate), each photograph was enlarged to nearly the same size image to give a direct comparison. Figures 19 to 23 are all for the same wing angle of attack, namely 18°, although as discussed there may be slight differences in the lift coefficients (the bound circulation).

The tip-vortex cross section for configuration 1 is shown in figure 19. It appears that the area inside the core of the vortex is turbulent and the core is surrounded by a potential flow which is in agreement with theory. The tip-vortex cross section for model configurations 2 and 3 are shown in figures 20 and 21, respectively. From these two figures no distinct vortex core is discernible as in figure 19. Further, from the tuft activity in the plane of the tuft grid it appears that some vorticity exists in this plane. Some of this tuft activity could be due to tunnel gustiness or slow camera shutter speed; however, it is unlikely this effect would show up in figures 20 and 21 and not in figure 19. It is possible that the vortex sheet is not completely rolled up. However, close comparison of figures 19(a) with 19(b) and 20(a) with 20(b) and also photographs taken at 9 chord lengths downstream do not reveal a noticeable decrease in the outer pseudocore turbulence. The vortex core can have axial and radial velocity components. Because of viscous forces, these velocity components result in vorticity in a plane perpendicular to the core axis (figs. 20 to 22). It is believed that the inplane vorticity for configurations 2 and 3 is a result of core axial velocity gradients that are insignificant in configuration 1. This additional vorticity is believed to be associated with the additional drag force encountered for configurations 2 and 3. The large increase in boundary-layer air associated with the

separation around the $5\frac{1}{2}$-in.-diameter (14 cm) disks did not seem to increase the core size. However the boundary-layer mass could still be contained in the vortex core, in accordance with reference 4, if the core axial velocity was increased proportionally. Therefore, it is concluded that while model configurations 2 and 3 did not appear to have any effect on the downstream vortex position, these configurations had an appreciable effect on the tip-vortex cross-sectional characteristics when compared with the plain tip (configuration 1).

Photographs of the vortex cross section for model configuration 4 (porous tip) are shown in figure 22. From the photographs, it can be seen that the core boundary is less discernible and also the area outside the core is more turbulent than for configurations 2 and 3.

The vortex cross section for model configuration 5 is shown in figure 23. This configuration is with a plain tip and a slotted cylinder with no blowing. Figure 23 indicates a vortex very similar to that of configuration 1 where a central turbulent core is present with a potential outer field. A preliminary review of the photographs with tip jet blowing did not reveal any large differences from figure 23.

CONCLUDING REMARKS

Wind-tunnel tests were performed on a semispan wing with rather radical wing-tip modifications. The tip modifications were chosen in an attempt to deform, displace, or modify the cross-sectional characteristics of the trailing tip vortex. These tests were performed at a Reynolds number of 2.6×10^6 and data were obtained up to 9 chord lengths behind the wing.

The tuft-grid-photographic system used in these tests to determine the vortex downstream displacement and cross-sectional characteristics proved satisfactory. This technique is recommended for further quantitative wind-tunnel testing.

No tip configuration was tested that resulted in any appreciable vortex core position change with respect to the basic (plain tip) configuration. This was in spite of the fact that the radical wing tips were chosen specifically to produce a change. One group of tip configurations that did not produce any noticeable downstream position change was that with tip jet blowing, with jet velocities up to five times free-stream velocities. These experimental results show that wing-tip modifications that do not grossly affect spanwise lift distribution will not produce a noticeable change in the position of the downstream tip vortex and these experimental results are in agreement with classical theory. Although the tip-vortex rolling-up process can start at or on the wing tip, the tip shape can affect the immediate rolling-up process; however, the results herein indicate that the downstream vortex position is not affected. This result is believed to be caused by the strong

potential associated with the lifting force being unaffected by relatively small tip force changes.

Tip-vortex cross-sectional variations were obtained with the wing-tip modifications. These cross-sectional variations indicate an increase in the turbulence in the flow field outside the core such that the outer field was no longer potential flow. In fact, in some cases, a vortex core boundary was not discernible. It is believed that the additional cross-sectional turbulence in the flow field outside the core is caused by axial velocity variations (along the free-stream direction) along the vortex radius. These velocity variations are attributed to the drag (axial momentum) associated with the wing-tip configuration modifications. Thus, the vortex cross-sectional variations were achieved at the expense of wing lift and/or drag characteristics. The blowing tip jet did not have any noticeable effect on the tip-vortex cross-sectional characteristics.

The experimental results herein indicate that for the plain wing tip the core diameter increased proportional to the square root of the downstream distance. Further, the core diameter increased in direct proportion with the lift coefficient. Both these conclusions agree with theory. A sample comparison shows that the experimental tangential velocity distribution agrees reasonably well with a theoretical distribution.

Langley Research Center,
National Aeronautics and Space Administration,
Hampton, Va., October 20, 1970.

REFERENCES

1. Clark, David R.; and Leiper, Albert C.: A Free Wake Analysis – A Method for the Prediction of Helicopter Rotor Hovering Performance. No. 321, 25th Annual National Forum Proceedings, Amer. Helicopter Soc., Inc., May 1969.

2. Spivey, Richard F.: Blade Tip Aerodynamics – Profile and Planform Effects. No. 205, 24th Annual National Forum Proceedings, Amer. Helicopter Soc., Inc., May 1968.

3. Sternfeld, H., Jr.: Influence of the Tip Vortex on Helicopter Rotor Noise. Fluid Dynamics of Rotor and Fan Supported Aircraft at Subsonic Speeds, AGARD CP No. 22, Sept. 1967, pp. 23/1-23/20.

4. McCormick, Barnes W.; Tangler, James L.; and Sherrieb, Harold E.: Structure of Trailing Vortices. J. Aircraft, vol. 5, no. 3, May-June 1968, pp. 260-267.

5. Smith, H. C.: Effects of a Porous Wingtip on an Aircraft Trailing Vortex. M.S. Thesis, Pennsylvania State Univ., 1967.

6. Smith, V. J.; and Simpson, G. J.: A Preliminary Investigation of the Effect of a Thin High Velocity Tip Jet on a Low Aspect Ratio Wing. Note ARL/A.163, Australia Dep. Supply, June 1957.

7. Spencer, R. H.; Sternfeld, H., Jr.; and McCormick, B. W.: Tip Vortex Core Thickening for Application to Helicopter Rotor Noise Reduction. USAAVLABS Tech. Rep. 66-1, U.S. Army, Sept. 1966. (Available from DDC as AD 644 317.)

8. Spreiter, John R.; and Sacks, Alvin H.: The Rolling Up of the Trailing Vortex Sheet and Its Effect on the Downwash Behind Wings. J. Aeronaut. Sci., vol. 18, no. 1, Jan. 1951, pp. 21-32, 72.

9. Dosanjh, D. S.; Gasparek, E. P.; and Eskinazi, S.: Decay of a Viscous Trailing Vortex. Aeronaut. Quart., vol. XIII, pt. 2, May 1962, pp. 167-188.

TABLE I.- CHARACTERISTICS OF MODEL CONFIGURATIONS 1 TO 4

Wing Geometry

Chord, in. (cm)	35.5 (90.2)
Thickness, in. (cm)	5.312 (13.49)
Span, in. (cm)	62 (158)
Reference area, ft^2 (m^2)	15.28 (1.419)
Twist, deg	0

Airfoil Coordinates

Section, percent chord	Chordwise station		Distance from chord line to surface			
			Upper		Lower	
	in.	cm	in.	cm	in.	cm
0	0	0	0	0	0	0
1.25	.44	1.12	.72	1.83	.70	1.78
2.50	.89	2.26	1.00	2.54	.93	2.36
5.00	1.78	4.52	1.39	3.53	1.25	3.18
7.50	2.70	6.86	1.64	4.17	1.54	3.91
10.00	3.55	9.02	1.85	4.70	1.76	4.47
15.00	5.32	13.51	2.16	5.49	2.13	5.41
20.00	7.10	18.03	2.37	6.02	2.43	6.17
30.00	10.63	27.00	2.50	6.35	2.80	7.11
40.00	14.20	36.07	2.38	6.05	2.90	7.37
50.00	17.75	45.08	2.11	5.36	2.73	6.93
60.00	21.30	54.10	1.80	4.57	2.31	5.87
70.00	24.80	62.99	1.39	3.53	1.78	4.52
80.00	28.40	72.14	.98	2.49	1.16	2.95
90.00	31.90	81.03	.50	1.27	.60	1.52
95.00	33.70	85.60	.29	.74	.30	.76
100.00	35.50	90.17	.04	.10	.04	.10

TABLE II.- CHARACTERISTICS OF MODEL CONFIGURATION 5

Span, in. (cm)	60 (152)
Reference area, ft^2 (m^2)	14.79 (1.374)
Cylinder:	
Diameter, in. (cm)	1.75 (4.44)
Length, in. (cm)	21 (53.3)
Slot length, in. (cm)	17.5 (44.4)
Approximate slot width, in. (cm)	0.05 (0.13)

TABLE III.- JET OPERATING CONDITIONS

Jet angle, deg	Mass-flow rate		Jet coefficient, C_μ
	slugs/sec	kg/sec	
0	0.0046	0.0671	0.00702
0	.0141	.2058	.054
45	.0047	.0686	.00741
45	.0144	.2101	.0563
90	.0047	.0686	.00741
90	.0146	.2131	.0570

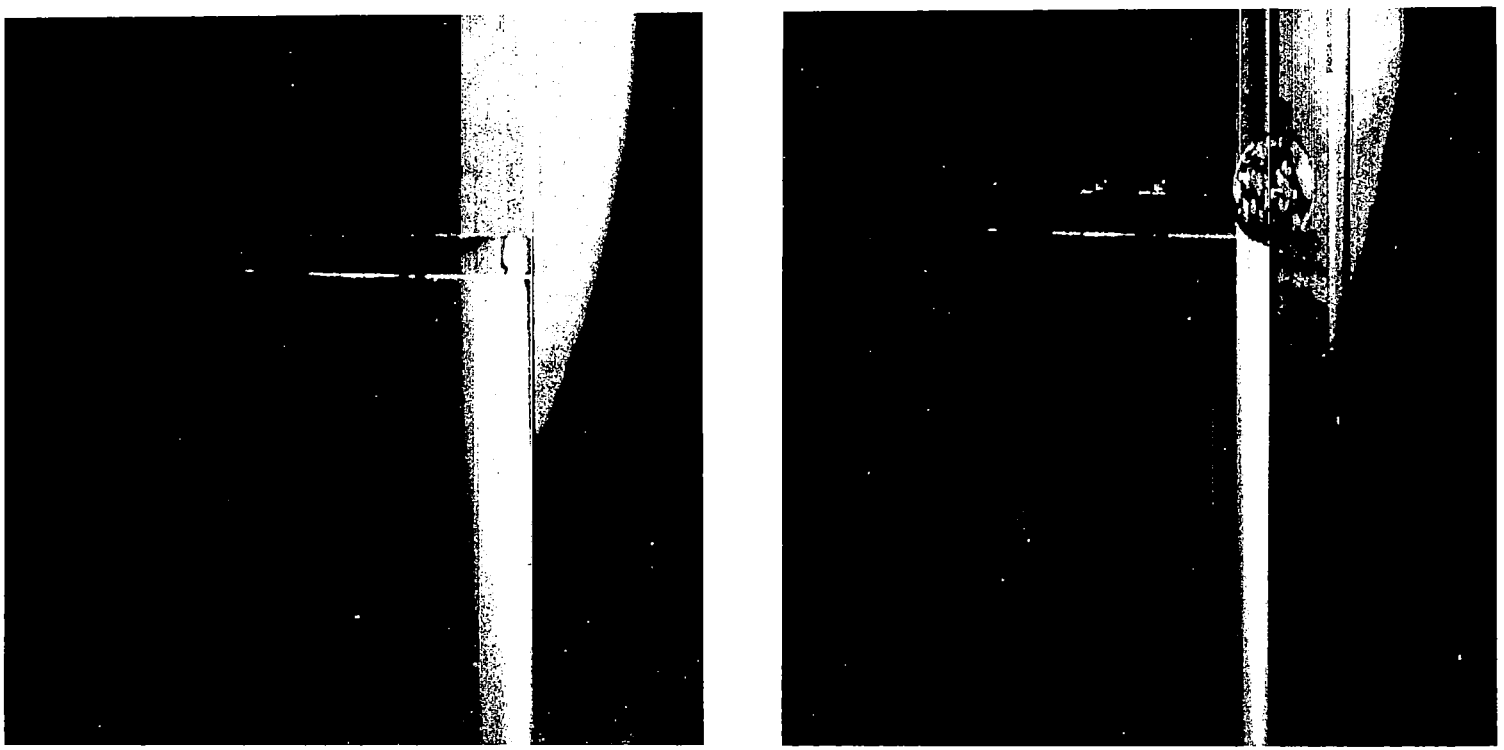

L-70-4787

(a) Configuration 1.

(b) Configuration 2.

Figure 1.- Configurations tested.

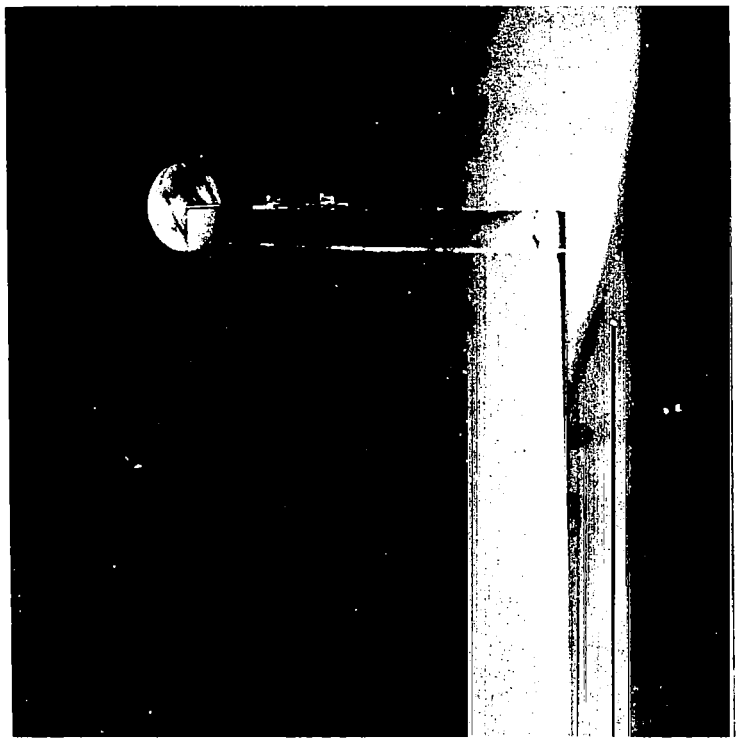

(c) Configuration 3.

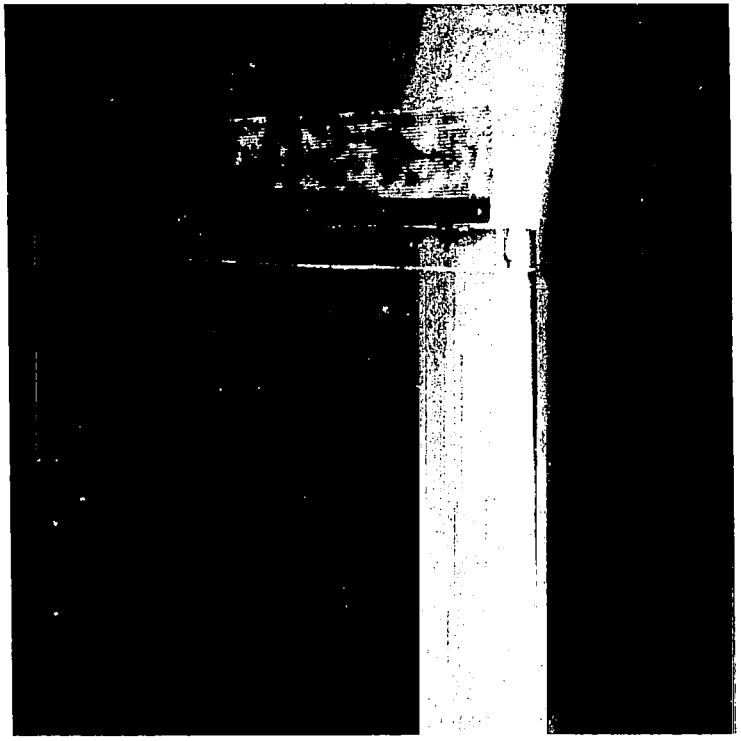

L-70-4788

(d) Configuration 4.

Figure 1.- Continued.

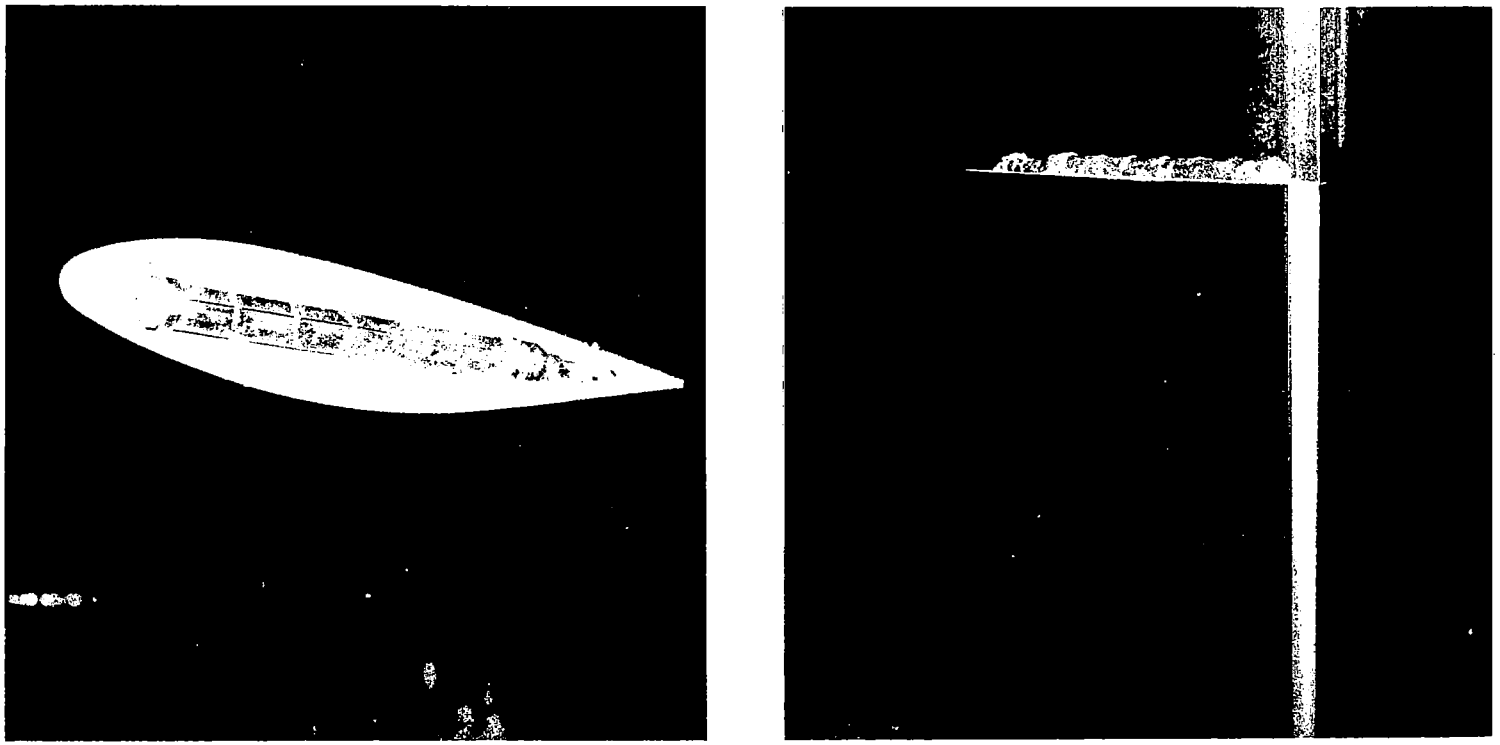

L-70-4789

(e) Configuration 5.

Figure 1.- Concluded.

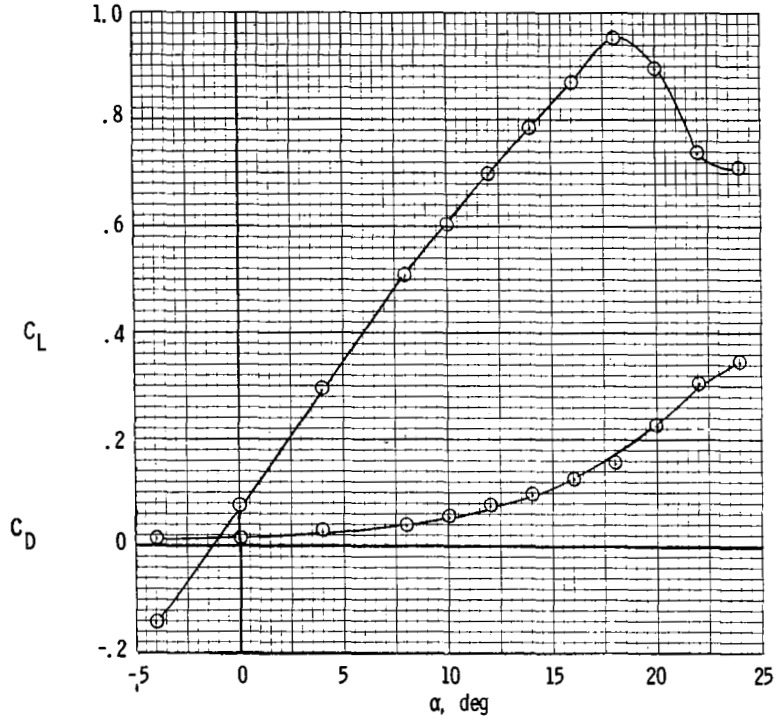

Figure 2.- Semispan wing lift and drag characteristics for configuration 1, plain wing tip (fig. 1(a)).

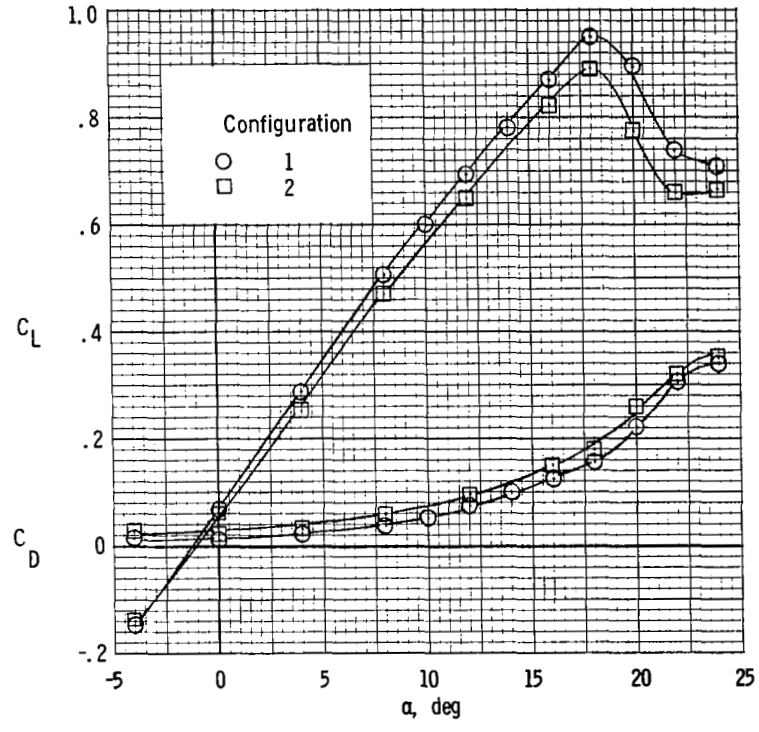

Figure 3.- Semispan wing lift and drag characteristics for configuration 2, leading-edge disk (fig. 1(b)).

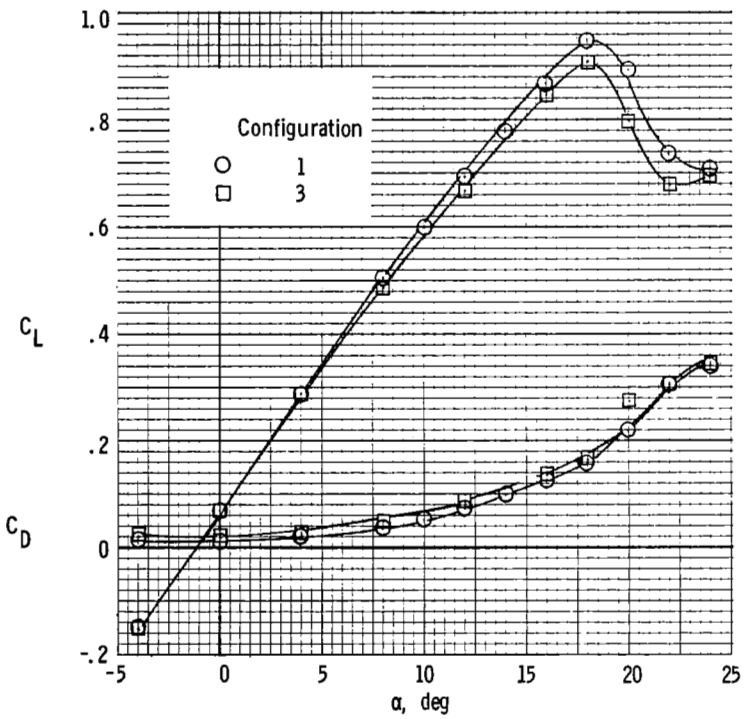

Figure 4.- Semispan wing lift and drag characteristics for configuration 3, trailing-edge disk (fig. 1(c)).

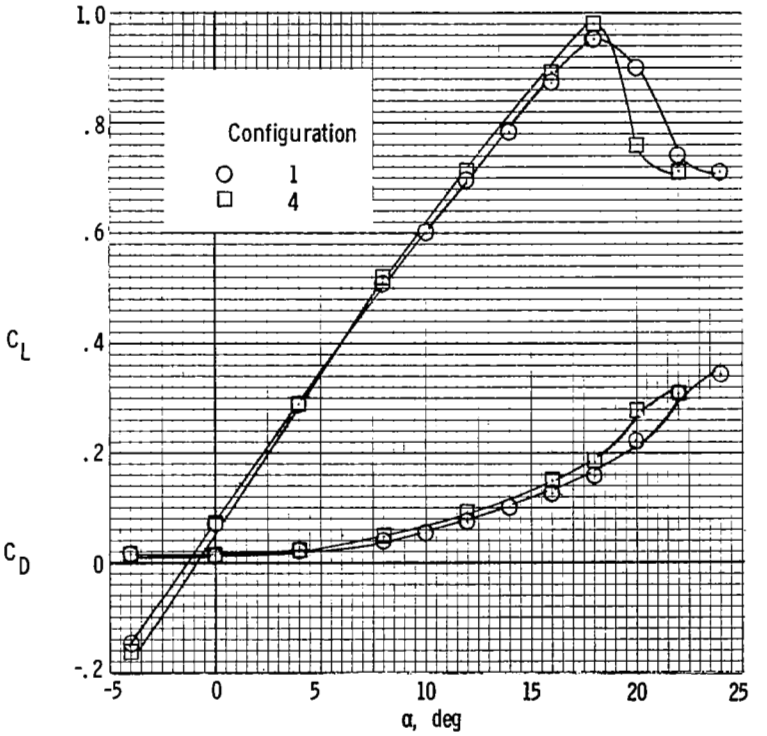

Figure 5.- Semispan wing lift and drag characteristics for configuration 4, perforated-plate tip (fig. 1(d)).

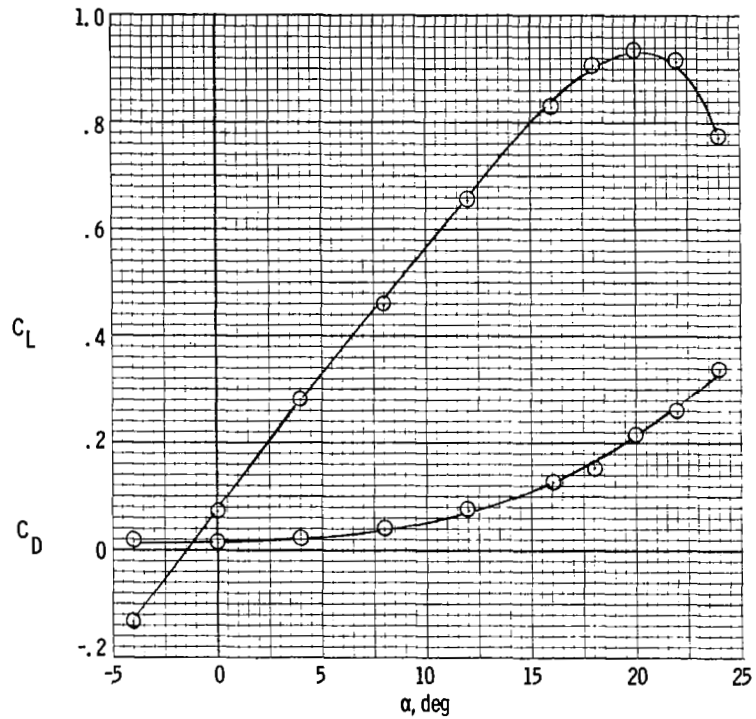

Figure 6.- Semispan wing lift and drag characteristics for configuration 5, zero jet mass flow (fig. 1(e)).

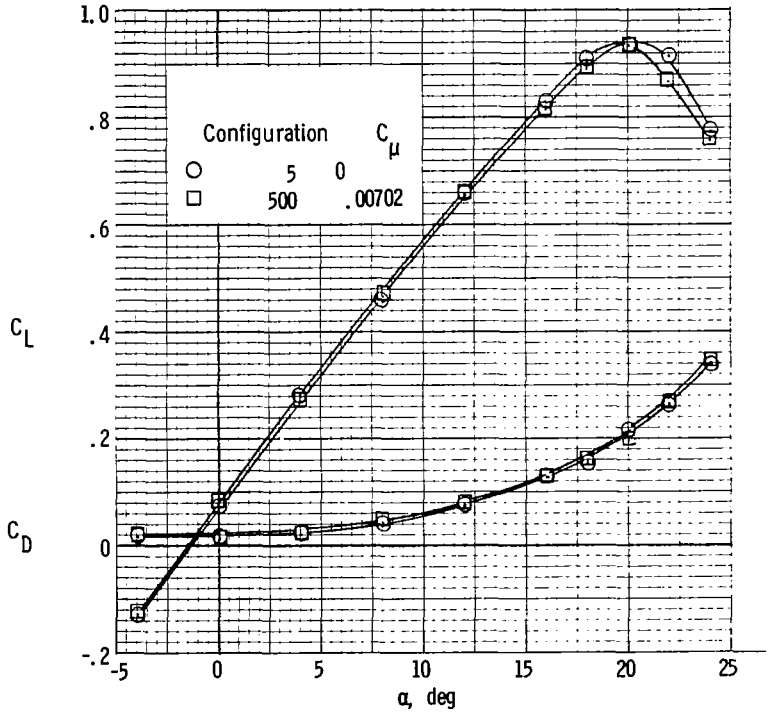

(a) Mass-flow rate of 0.0046 slug/sec (0.0671 kg/sec).

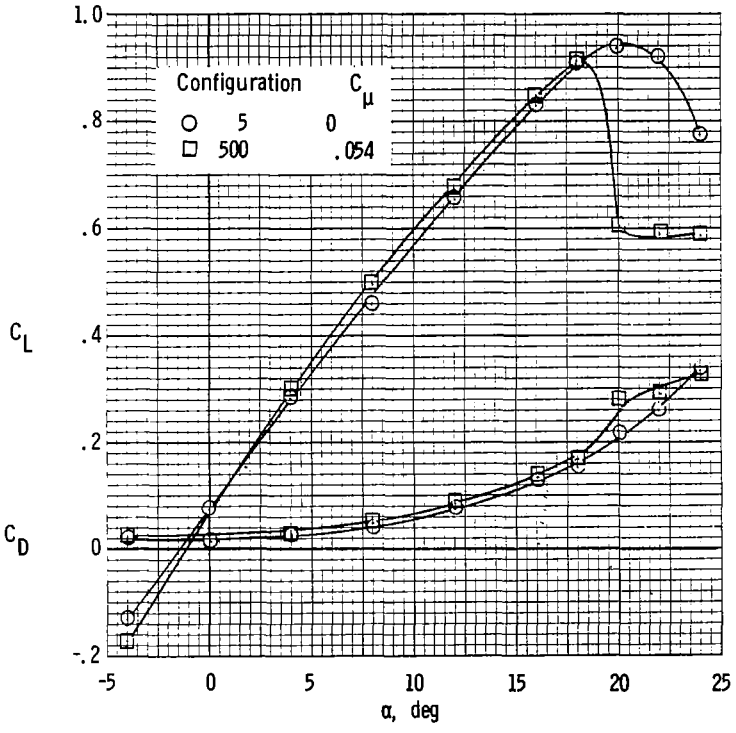

(b) Mass-flow rate of 0.0141 slug/sec (0.2058 kg/sec).

Figure 7.- Semispan wing lift and drag characteristics for configuration 500, spanwise jet blowing.

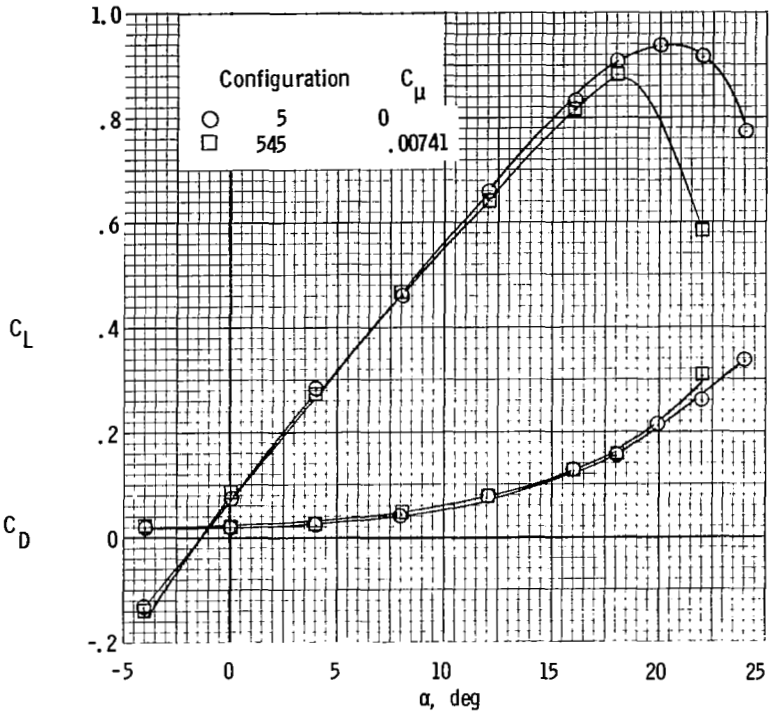

Figure 8.- Semispan wing lift and drag characteristics for configuration 545, jet blowing 45° from span axis. Mass-flow rate, 0.0047 slug/sec (0.0686 kg/sec).

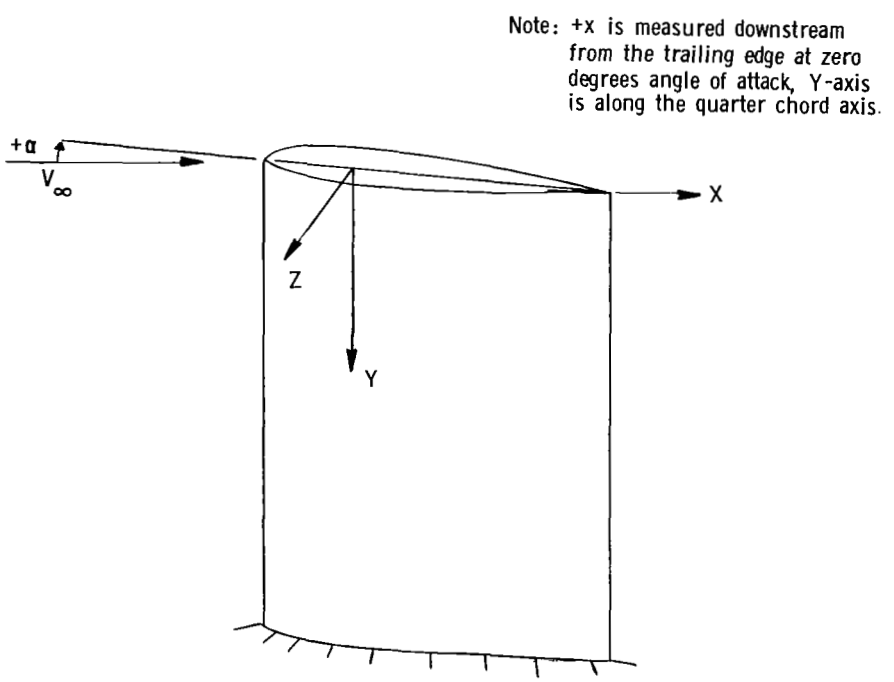

Figure 9.- Coordinate system used for defining the tip-vortex displacement.

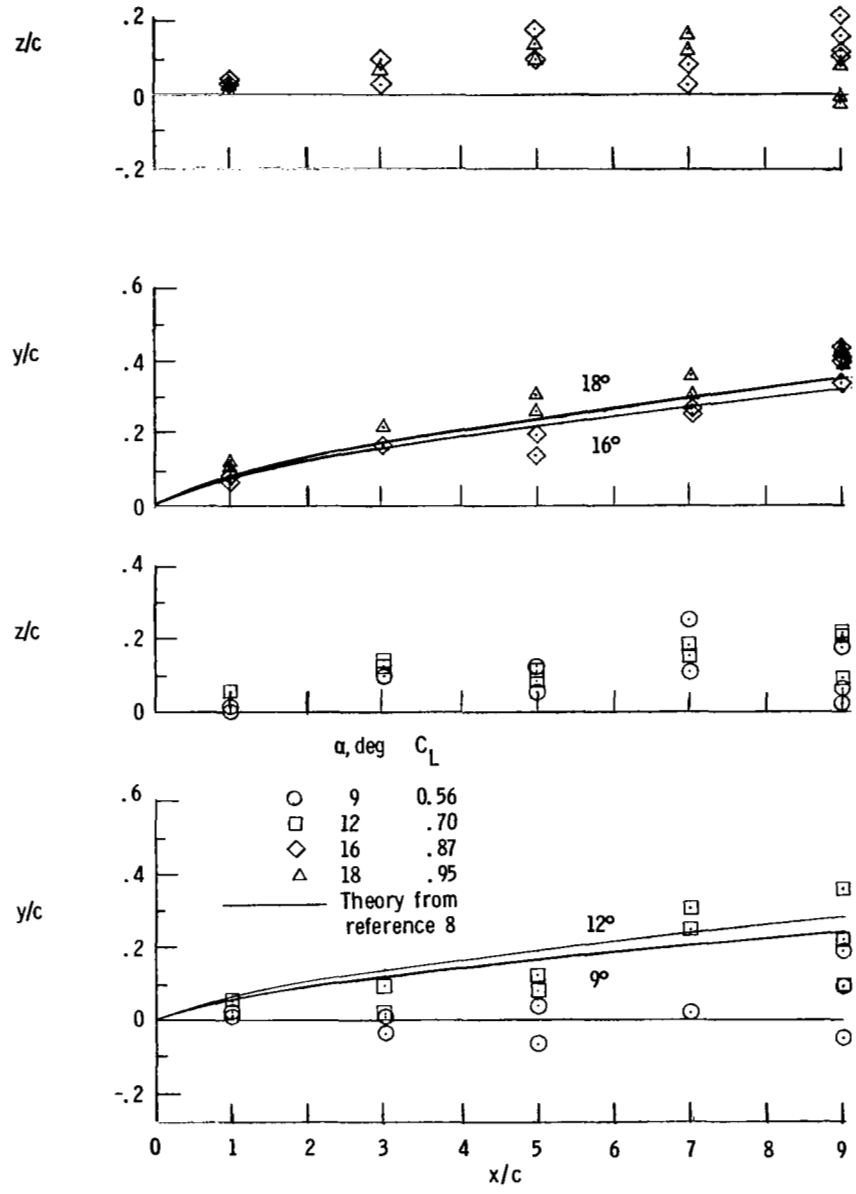

Figure 10.- Tip-vortex displacement for various angles of attack for basic semispan wing with the plain tip. Configuration 1.

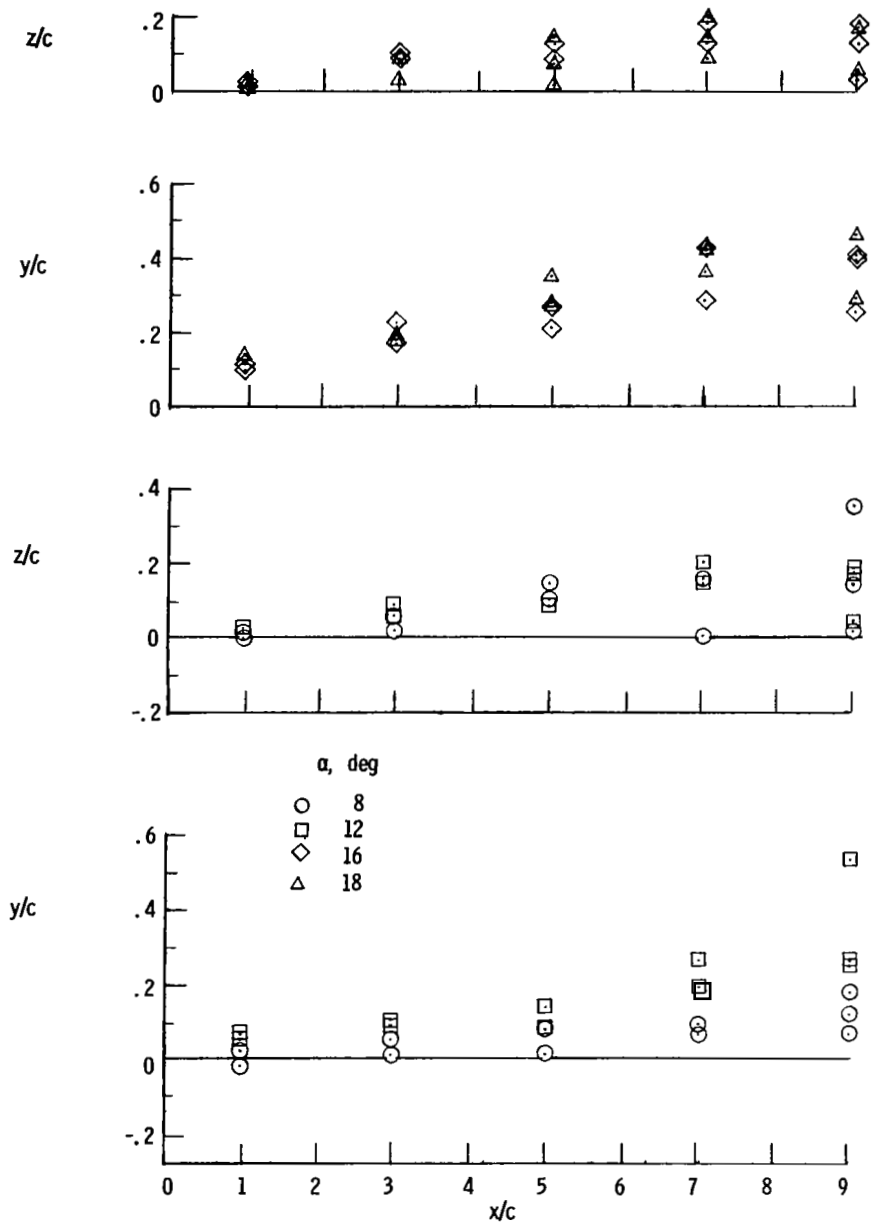

Figure 11.- Tip-vortex displacement for various angles of attack for the basic tip for jet blowing, zero jet flow rate. Configuration 500.

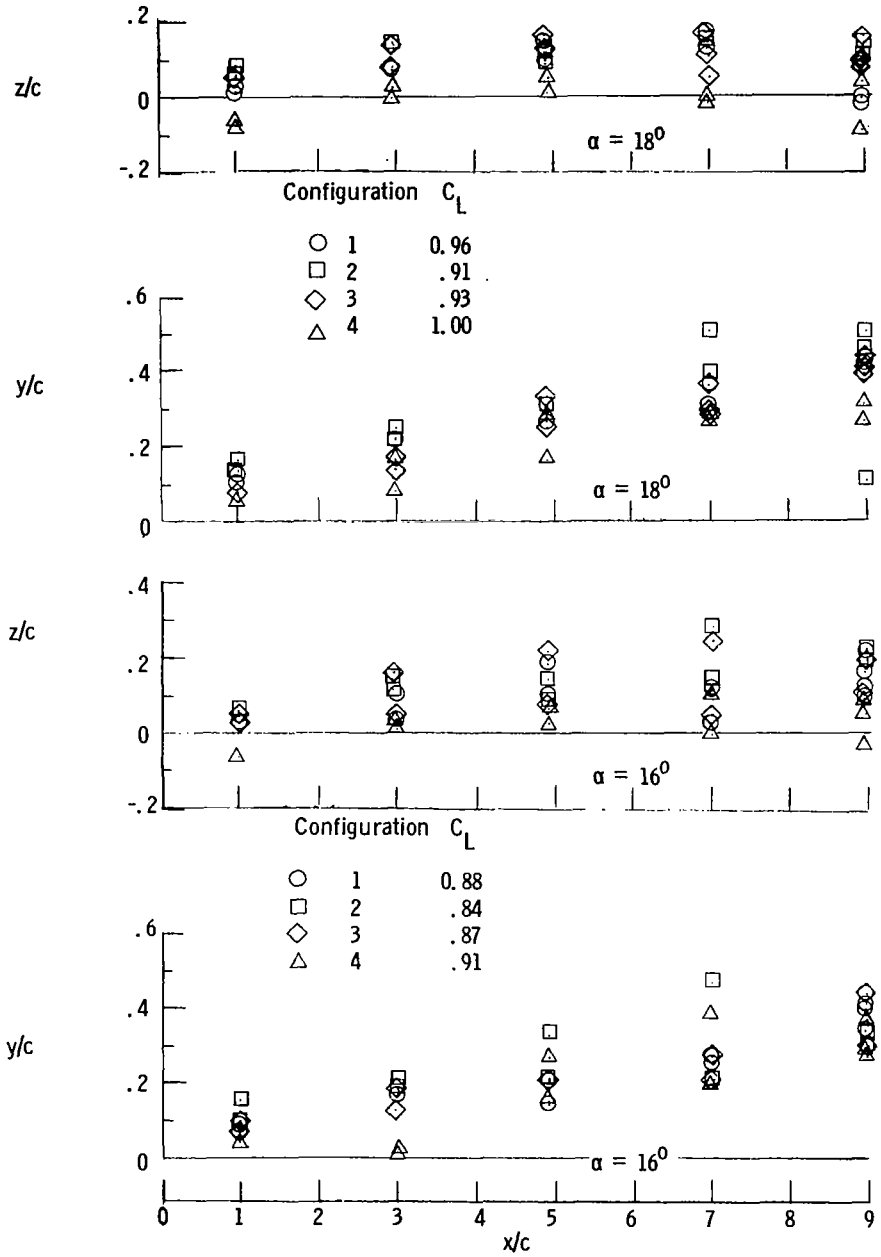

Figure 12.- Comparison of tip-vortex displacement for configurations 1 to 4. $\alpha = 16^{\circ}$ and 18°.

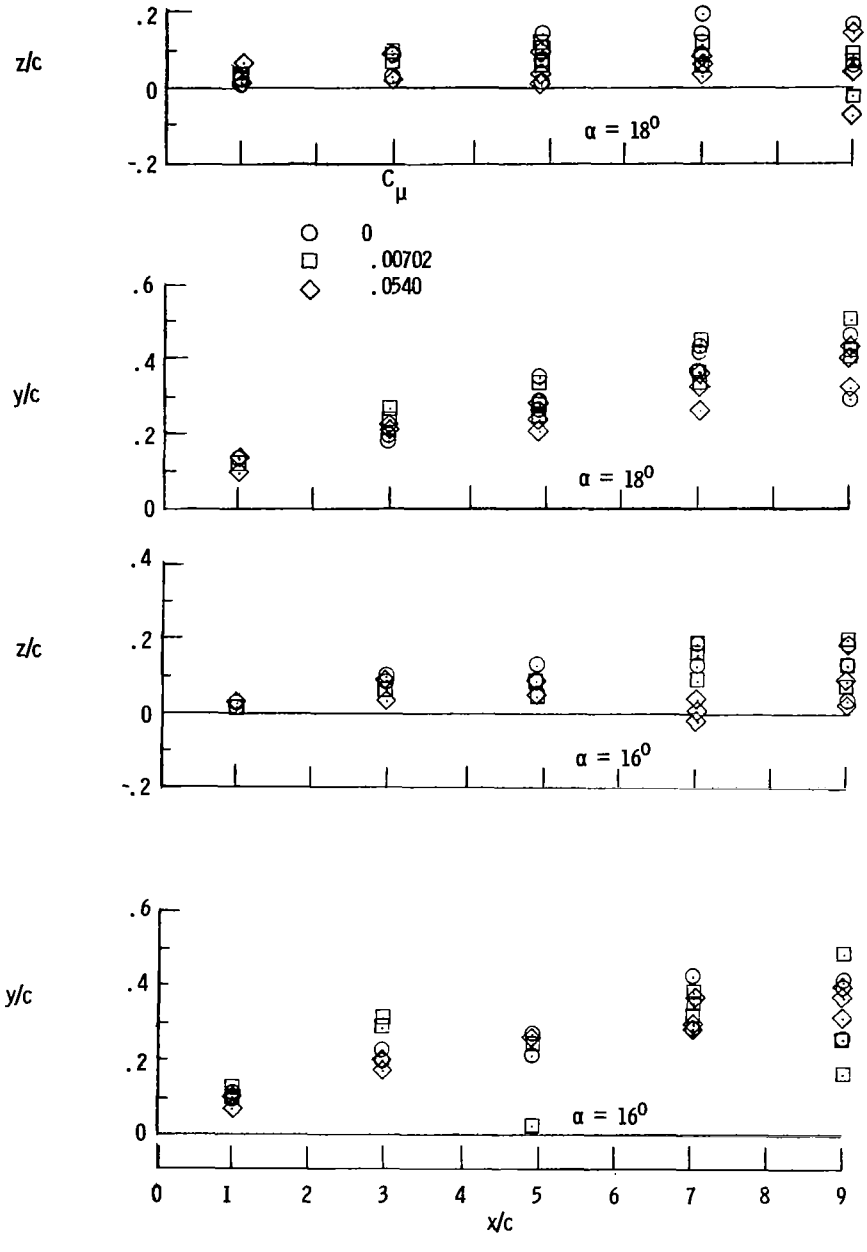

Figure 13.- Comparison of tip-vortex displacement for configuration 500 (spanwise blowing) with three jet mass-flow rates. $\alpha = 16^{o}$ and 18^{o}.

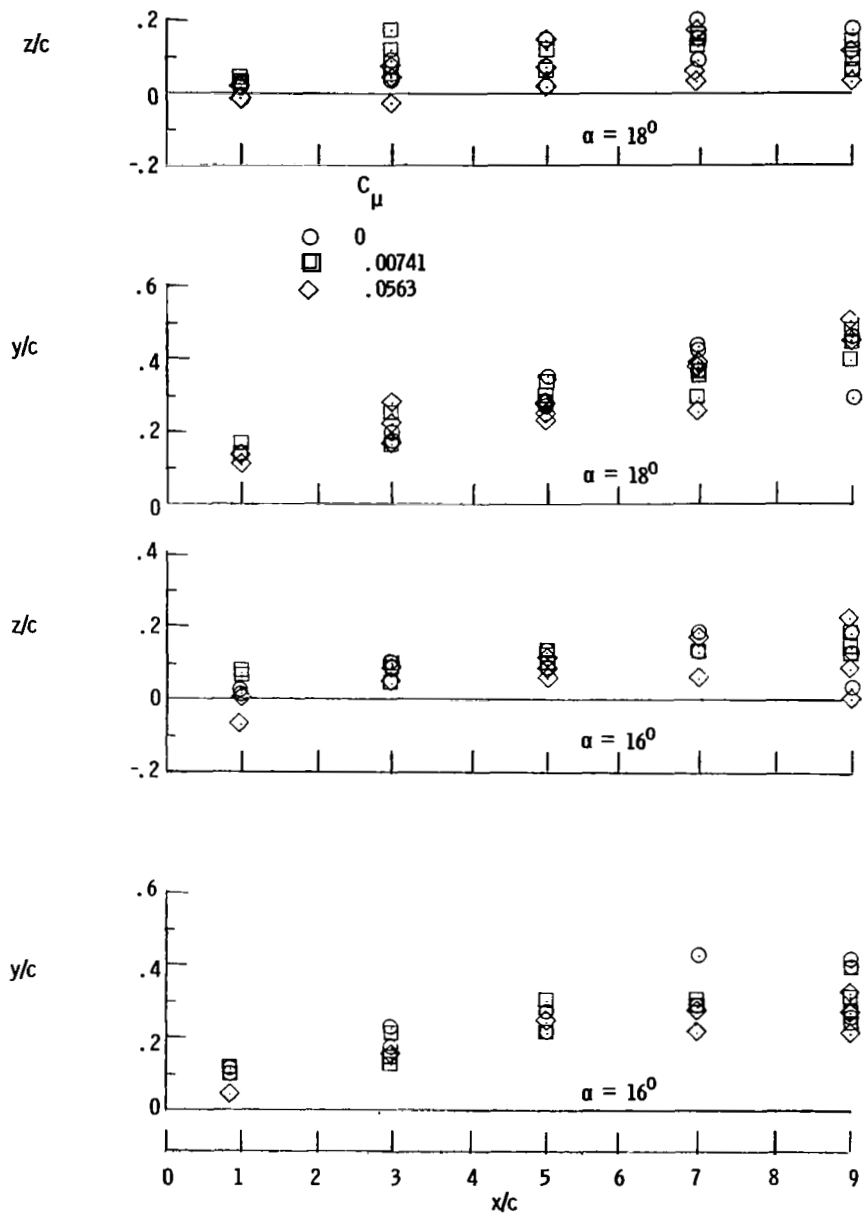

Figure 14.- Comparisons of tip-vortex displacement for configuration 5 (blowing downward 45° from span chord plane) with three jet mass-flow rates. α = 16° and 18°.

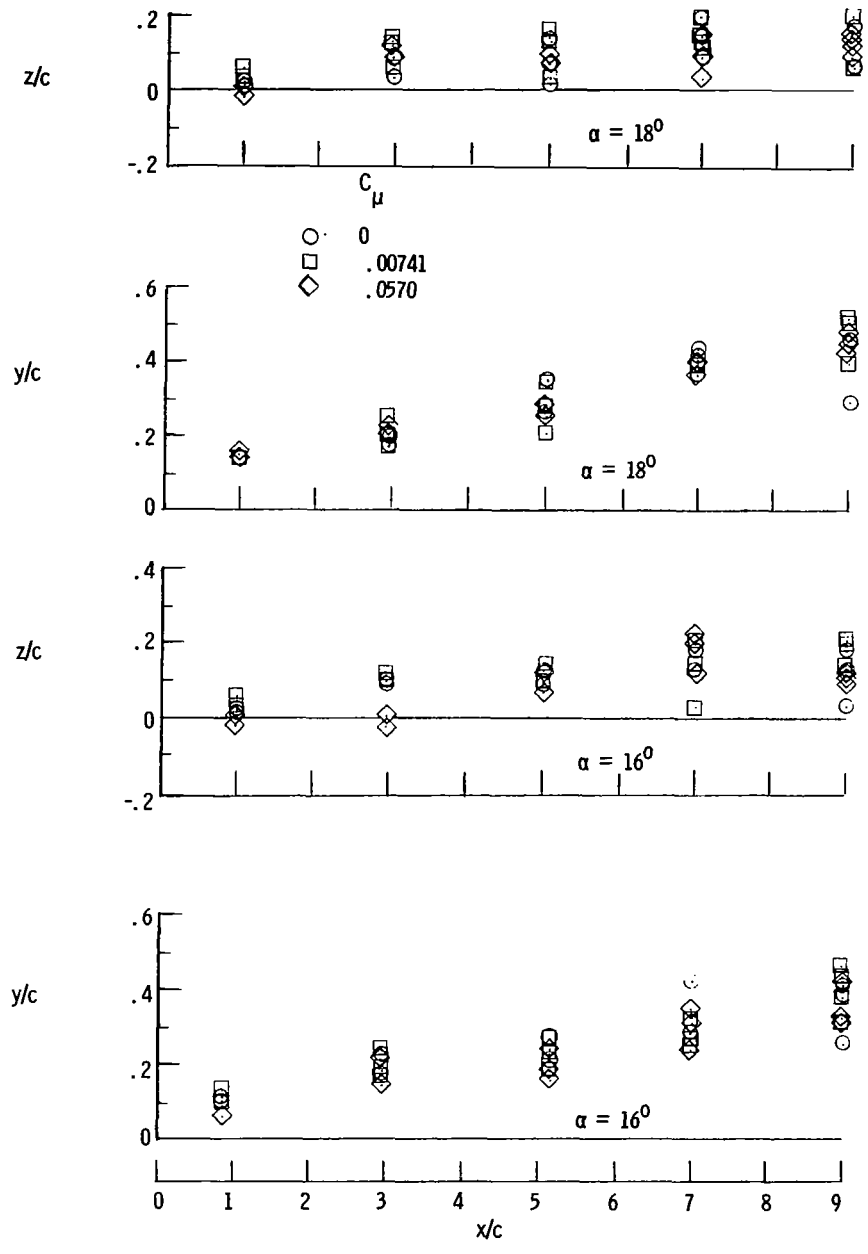

Figure 15.- Comparison of tip-vortex displacement for configuration 5 (blowing 90° downward from span chord plane) with three jet mass-flow rates. α = 16° and 18°.

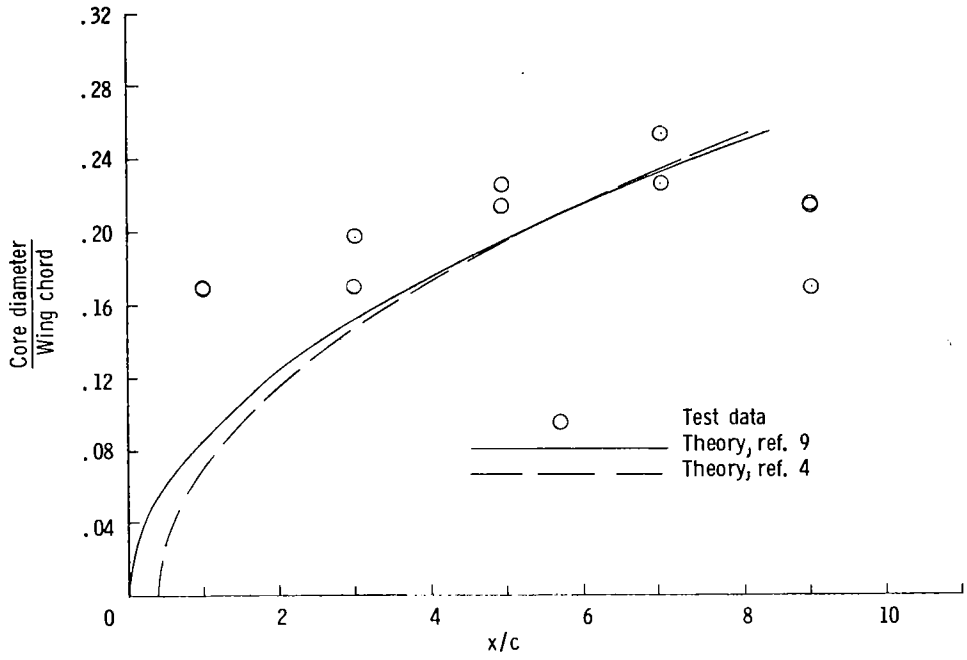

Figure 16.- Estimated vortex core size for configuration 1 for $C_L = 0.87$. $\alpha = 16^o$.

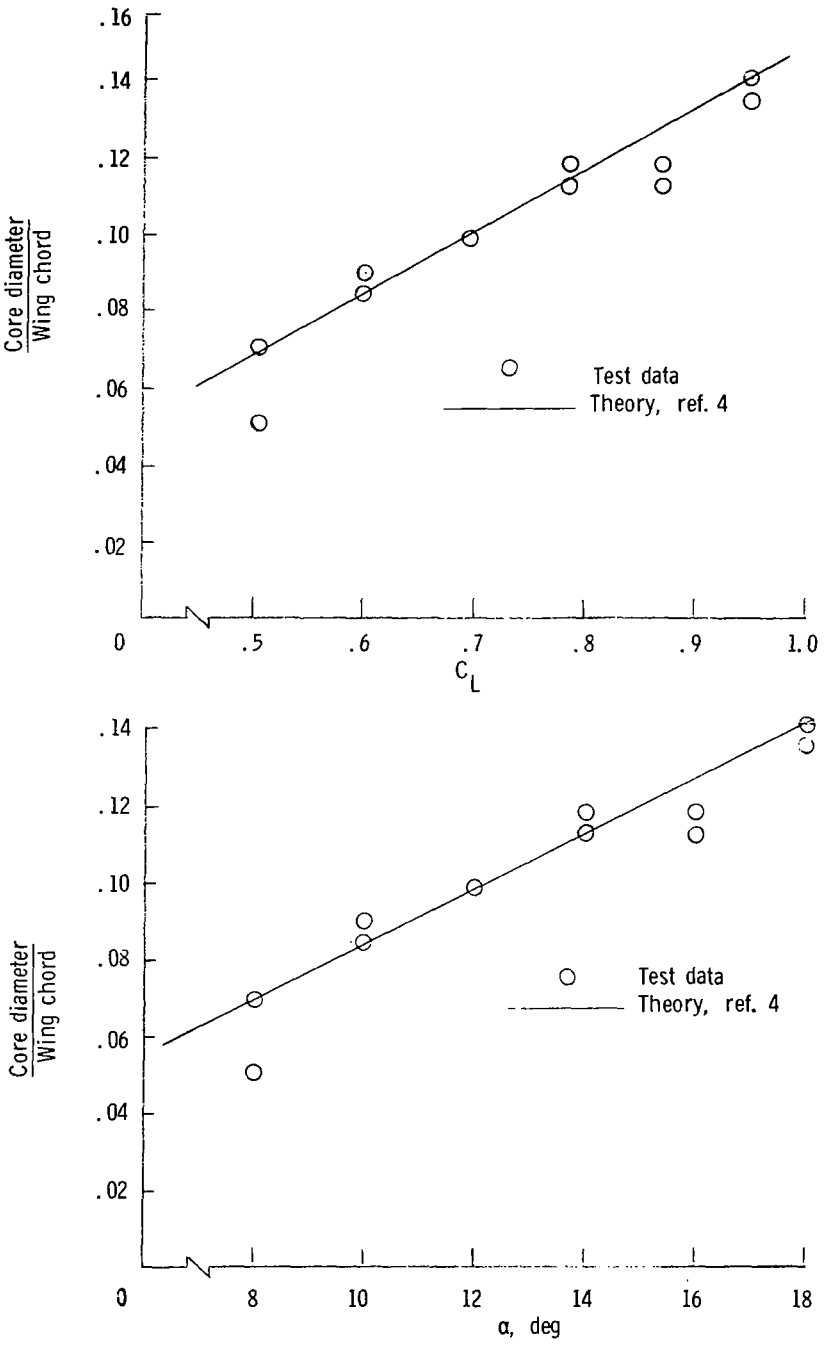

Figure 17.- Estimated vortex core size for configuration 1 at 5 chord lengths downstream.

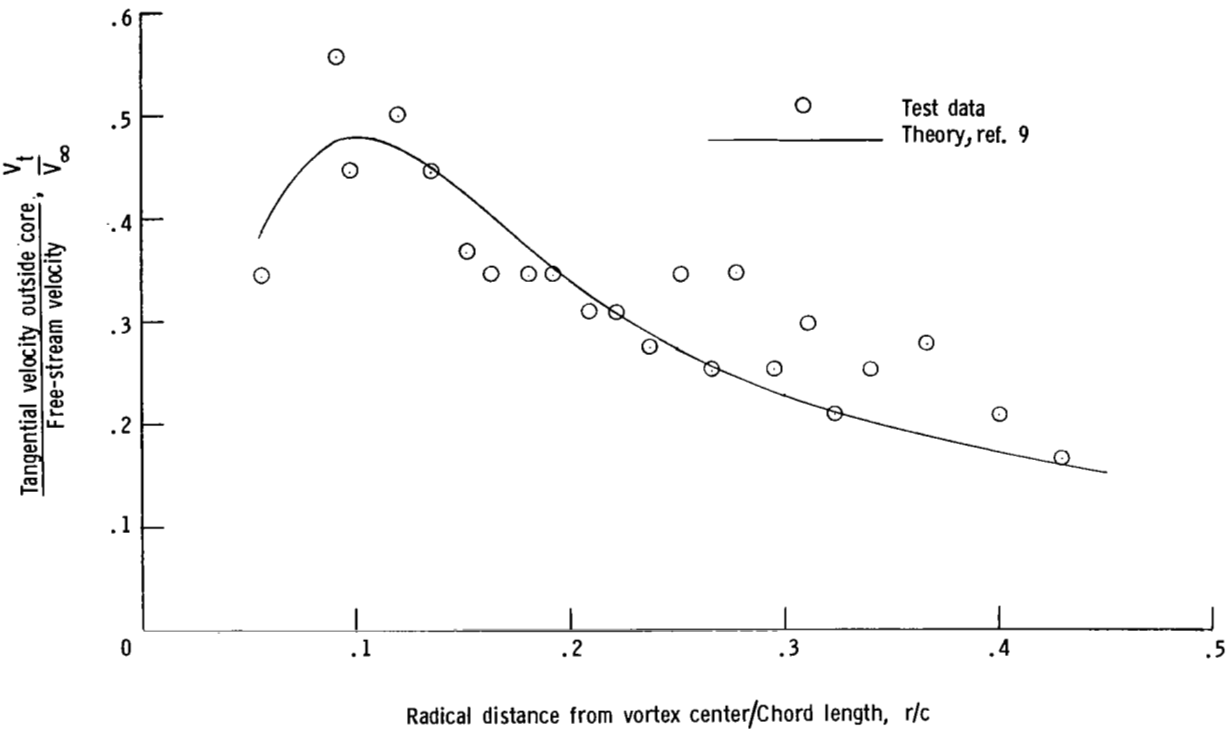

Figure 18.- Tangential velocity distribution of the vortex for configuration 1 at $\alpha = 8^{o}$ and 5 chord lengths downstream.

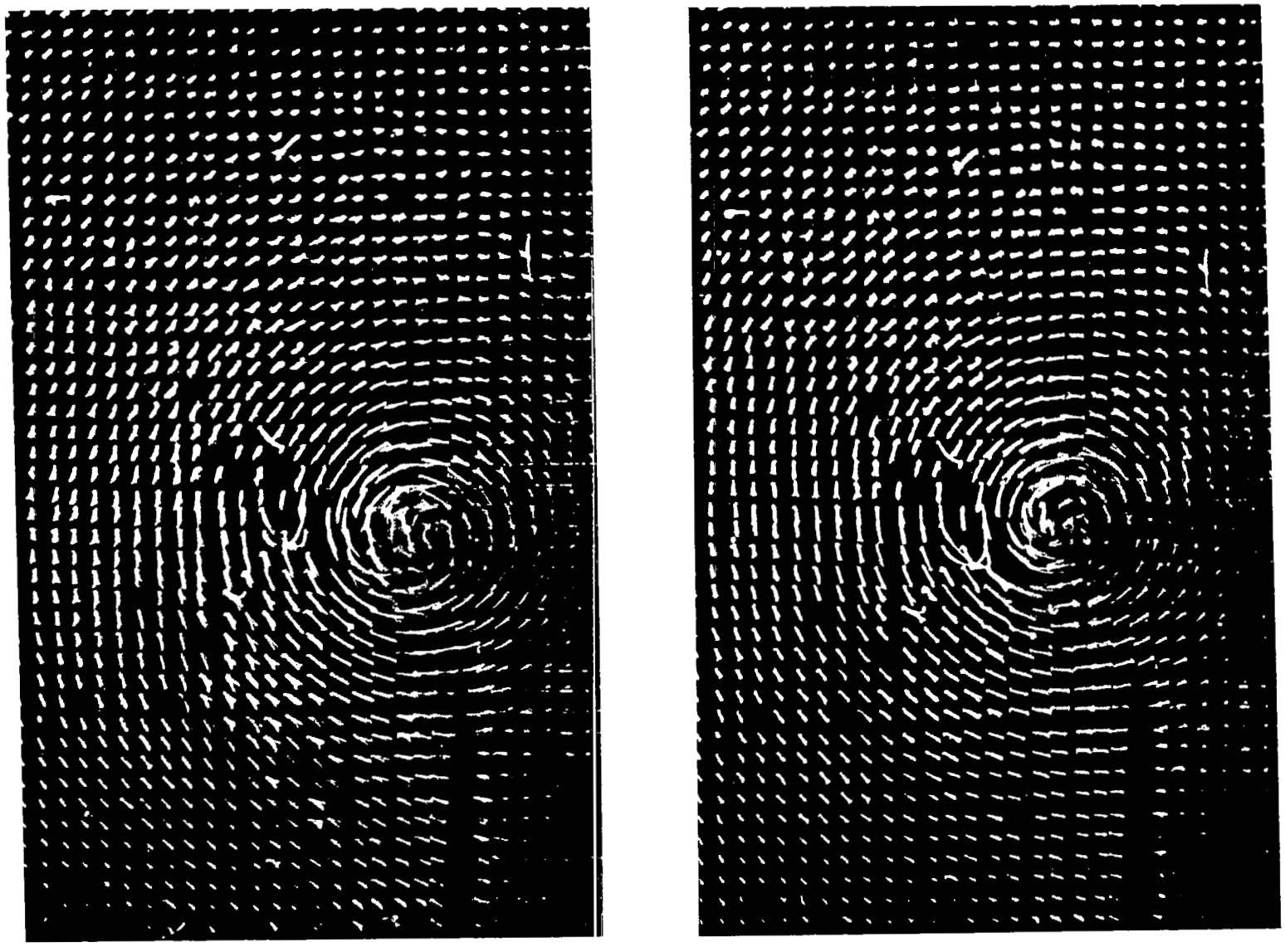

(a) 5 chord lengths downstream.

Figure 19.- Tip-vortex cross-sectional characteristics for configuration 1. $\alpha = 18^{o}$; 1-in. (2.54 cm) grid spacing.

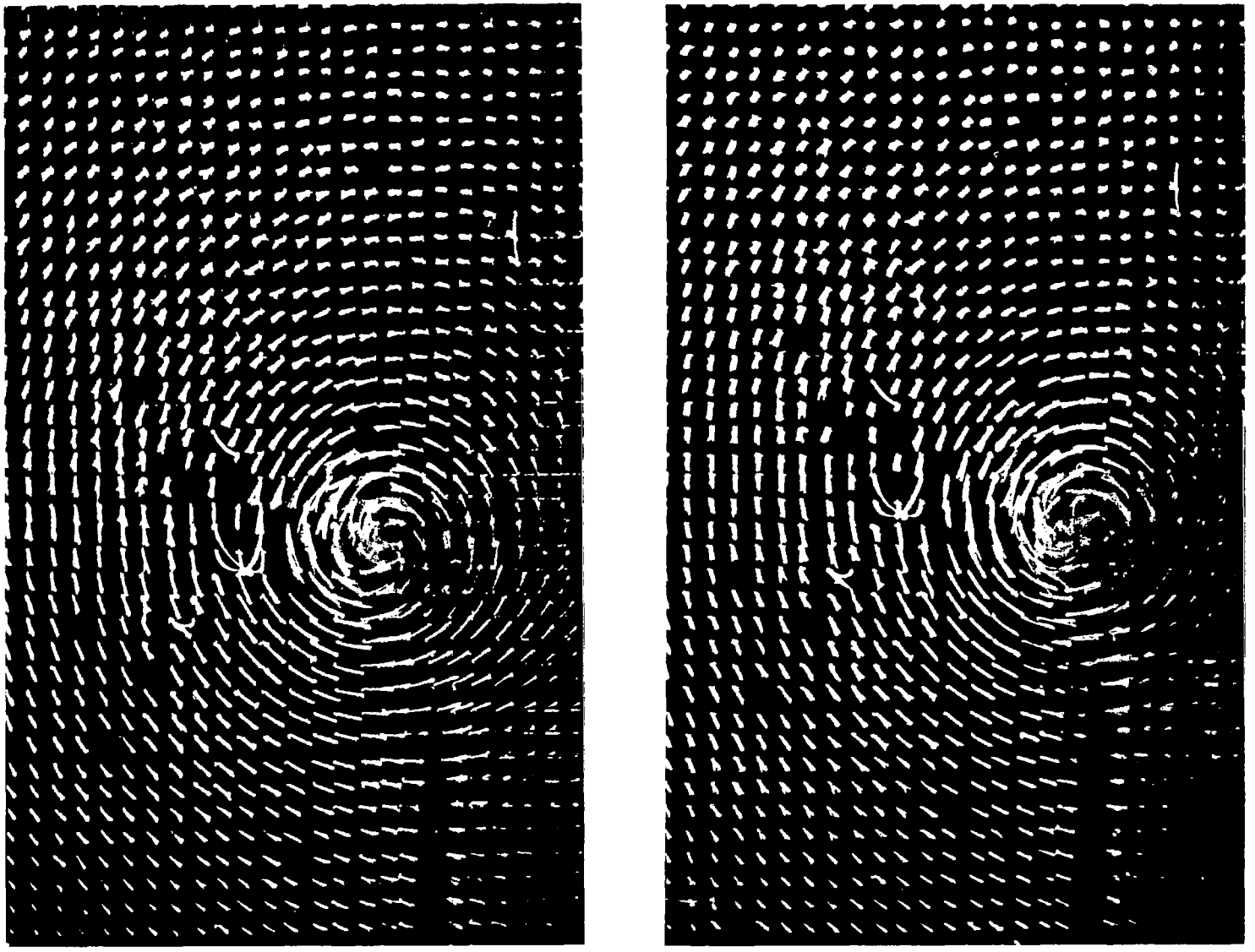

(b) 7 chord lengths downstream.

Figure 19.- Concluded.

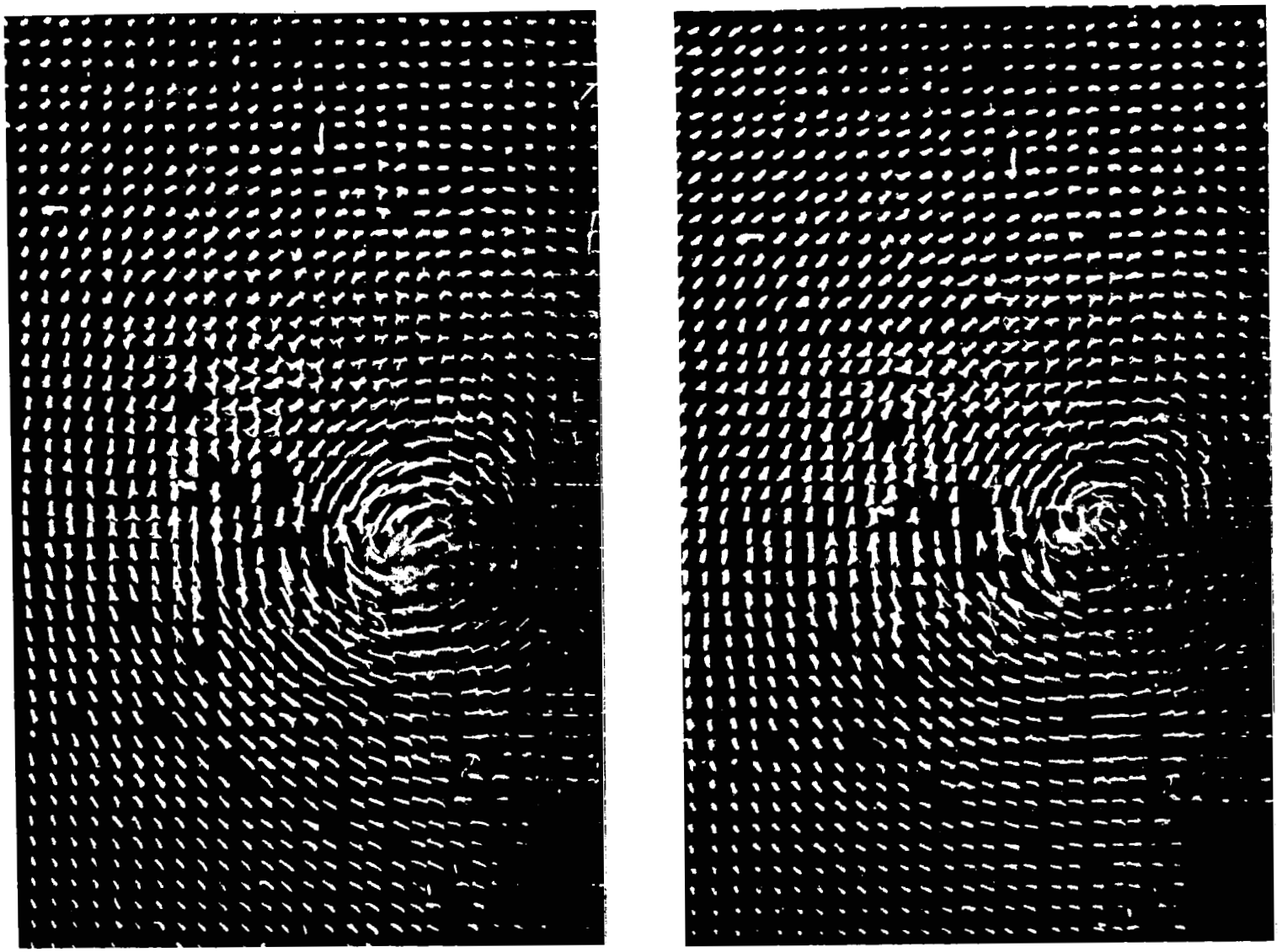

(a) 5 chord lengths downstream.

Figure 20.- Tip-vortex cross-sectional characteristics for configuration 2. $\alpha = 18^{o}$; 1-in. (2.54 cm) grid spacing.

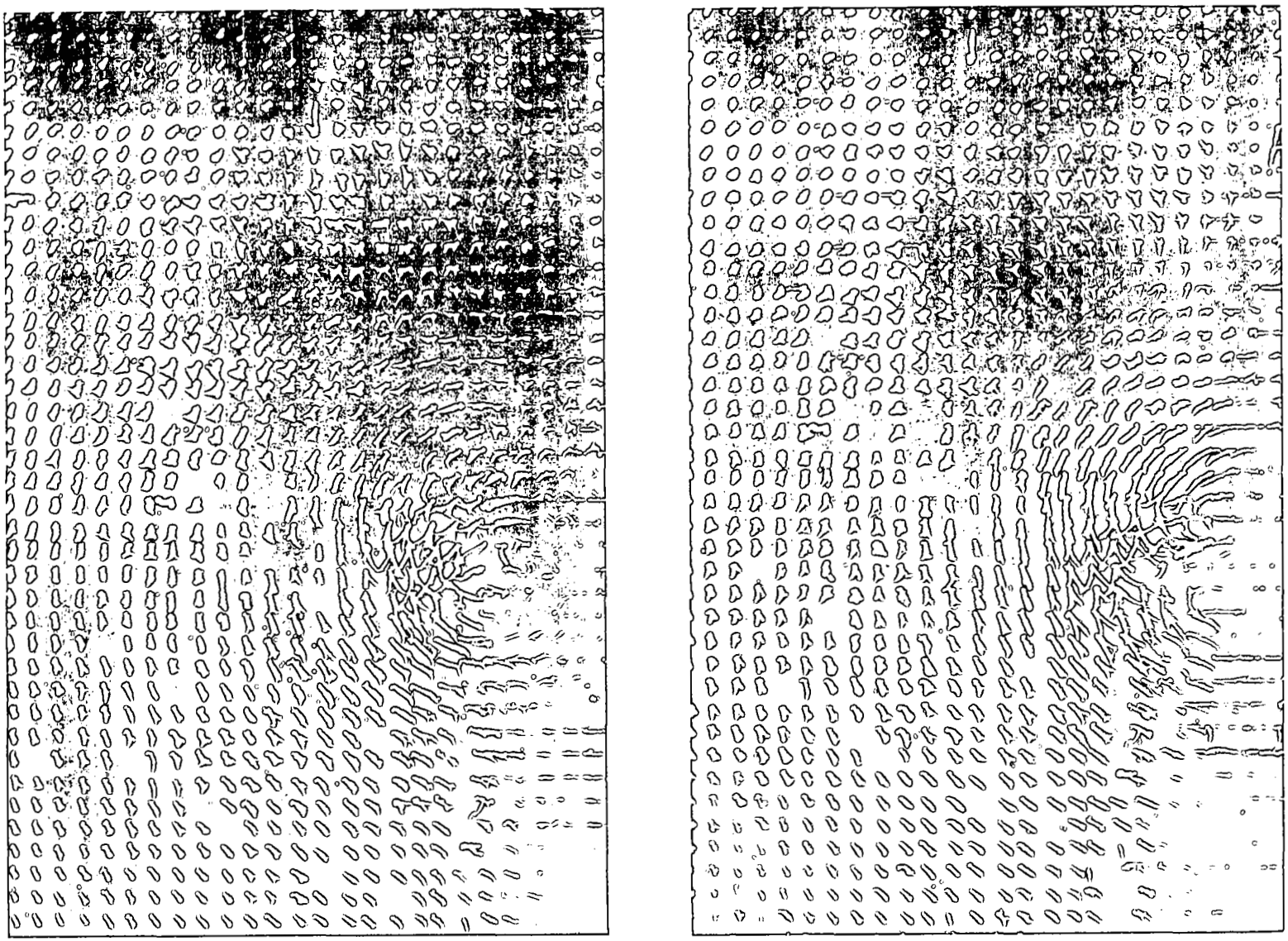

(b) 7 chord lengths downstream.

Figure 20.- Concluded.

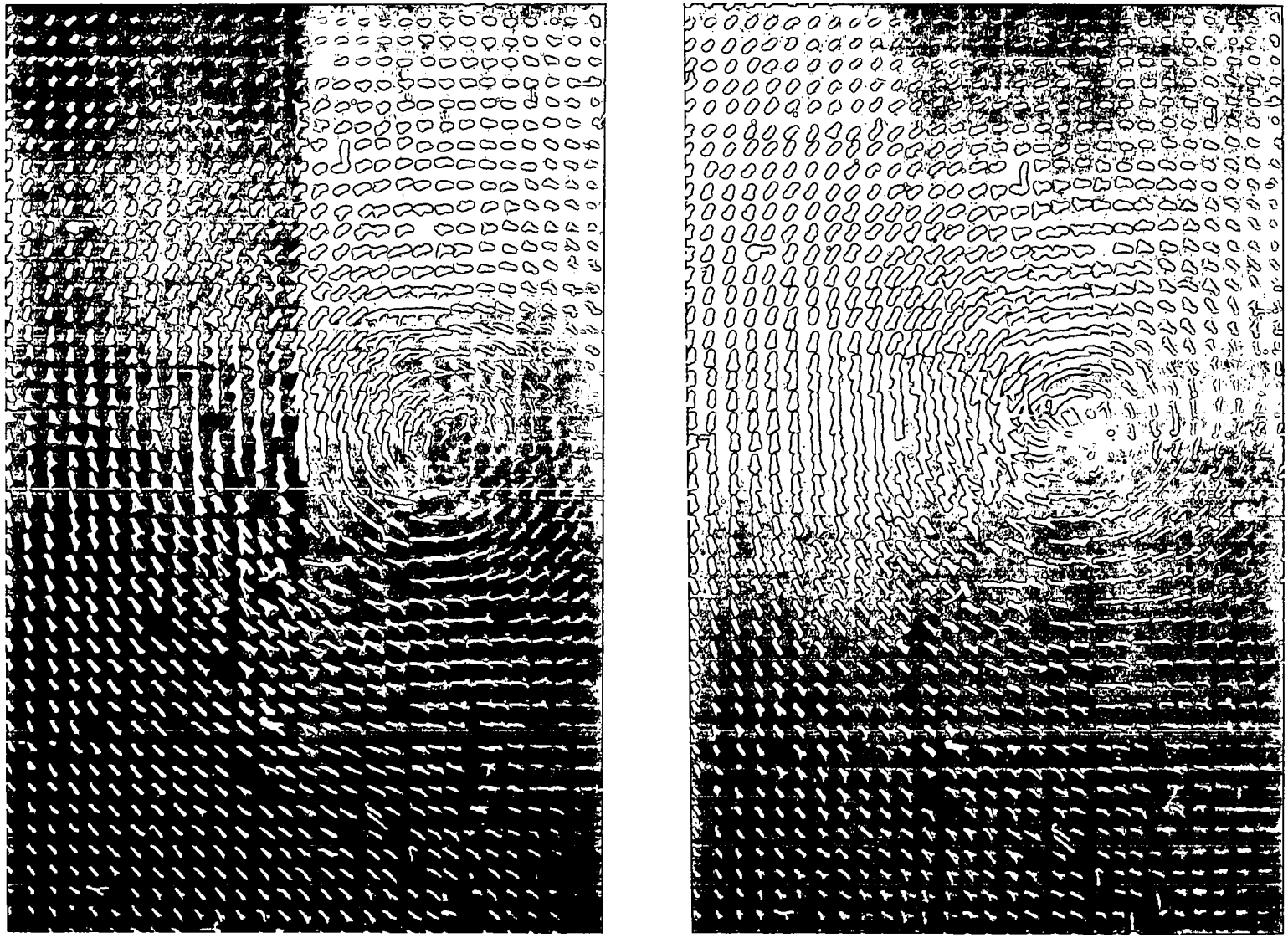

(a) 5 chord lengths downstream.

Figure 21.- Tip-vortex cross-sectional characteristics for configuration 3. $\alpha = 18^{o}$; 1-in. (2.54 cm) grid spacing.

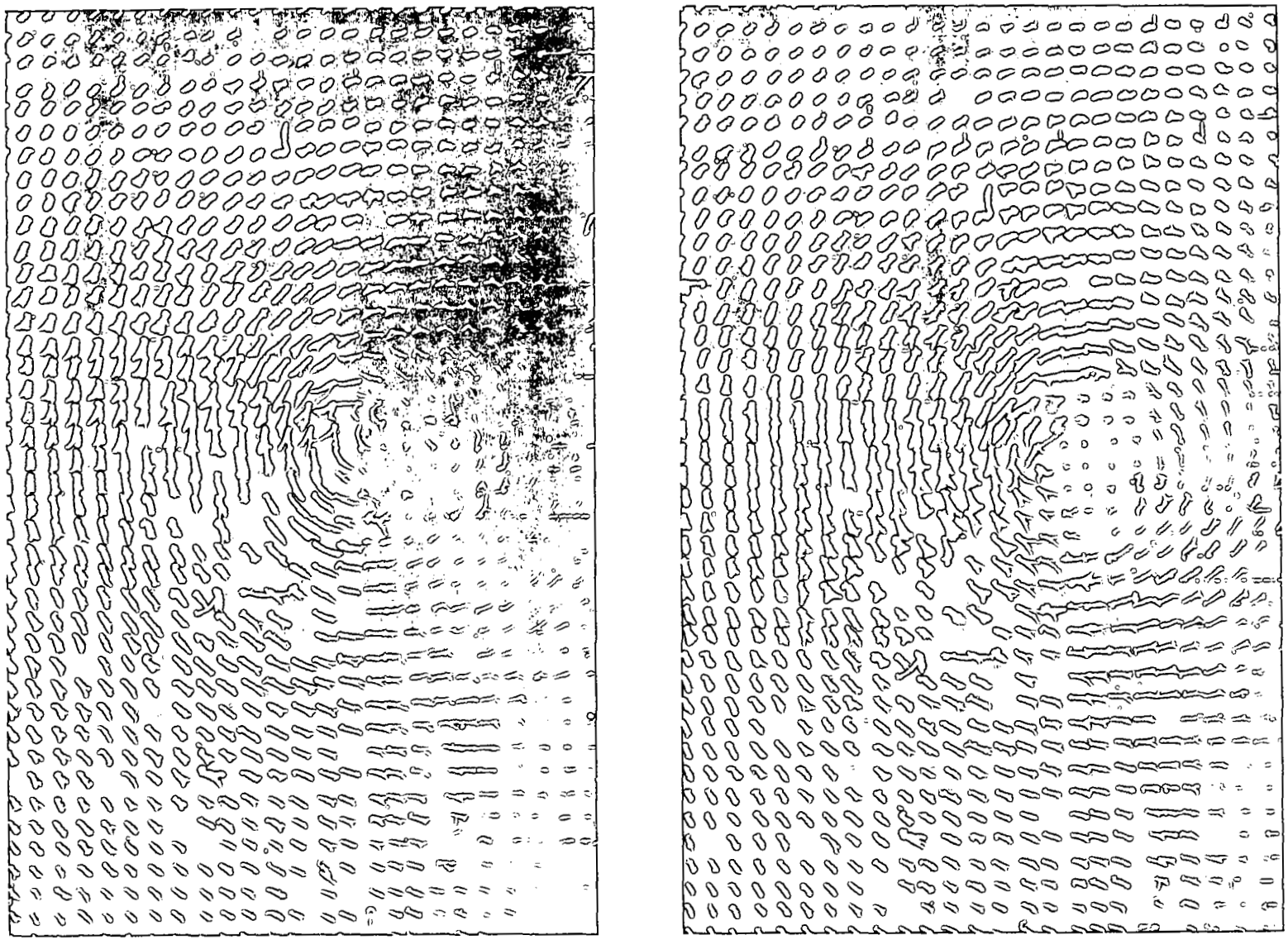

(b) 7 chord lengths downstream.

Figure 21.- Continued.

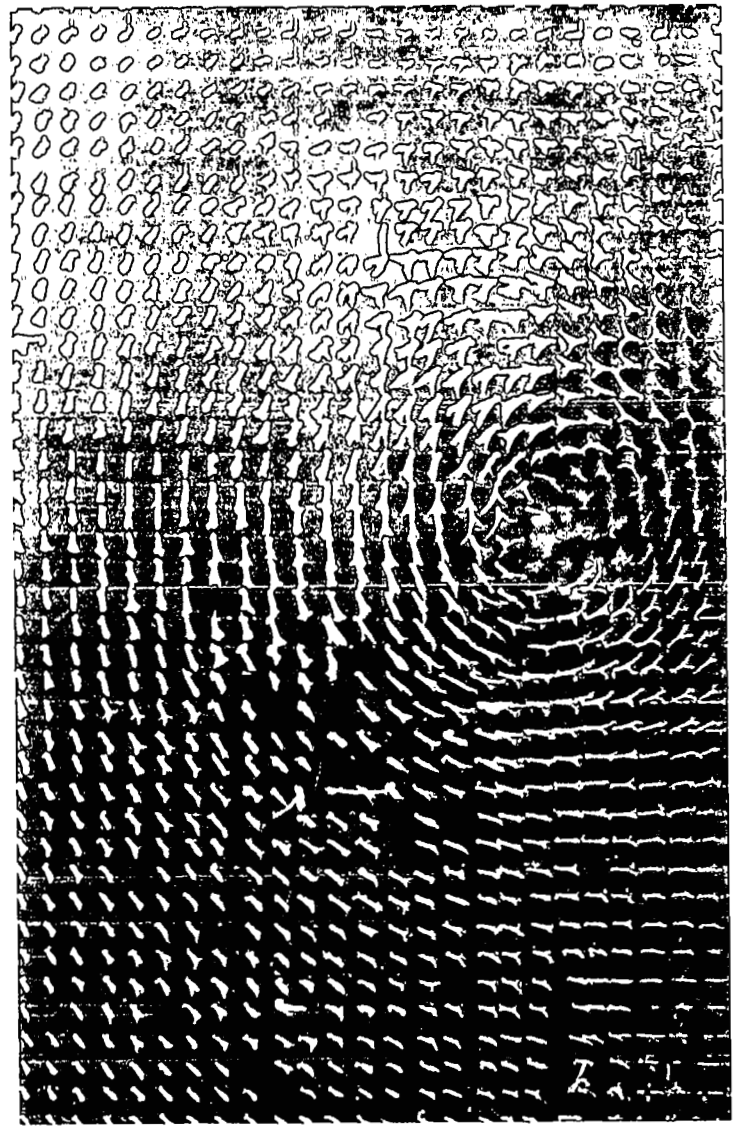

(b) Concluded.

Figure 21.- Concluded.

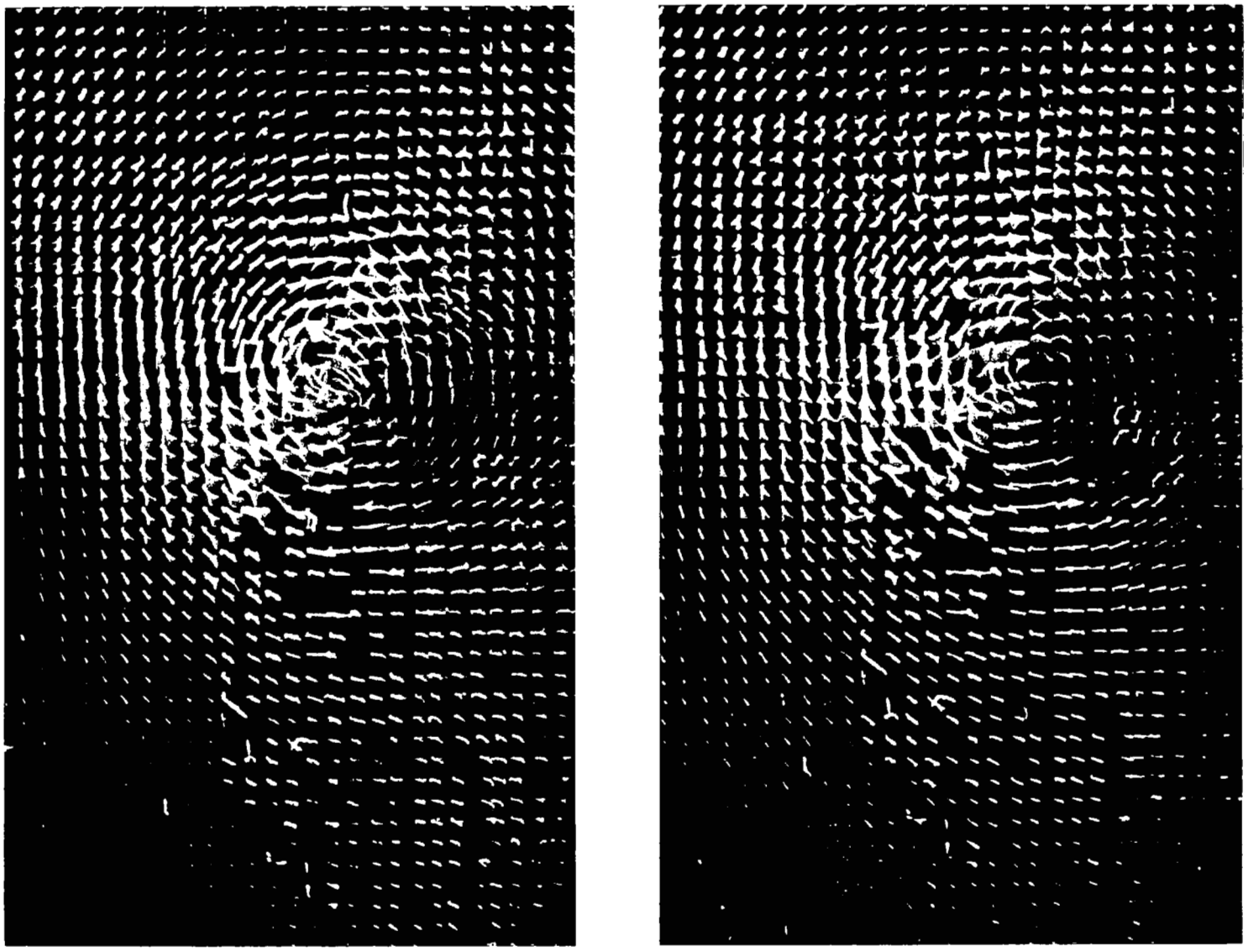

(a) 5 chord lengths downstream.

Figure 22.- Tip-vortex cross-sectional characteristics for configuration 4. $\alpha = 18^{\circ}$; 1-in. (2.54 cm) grid spacing.

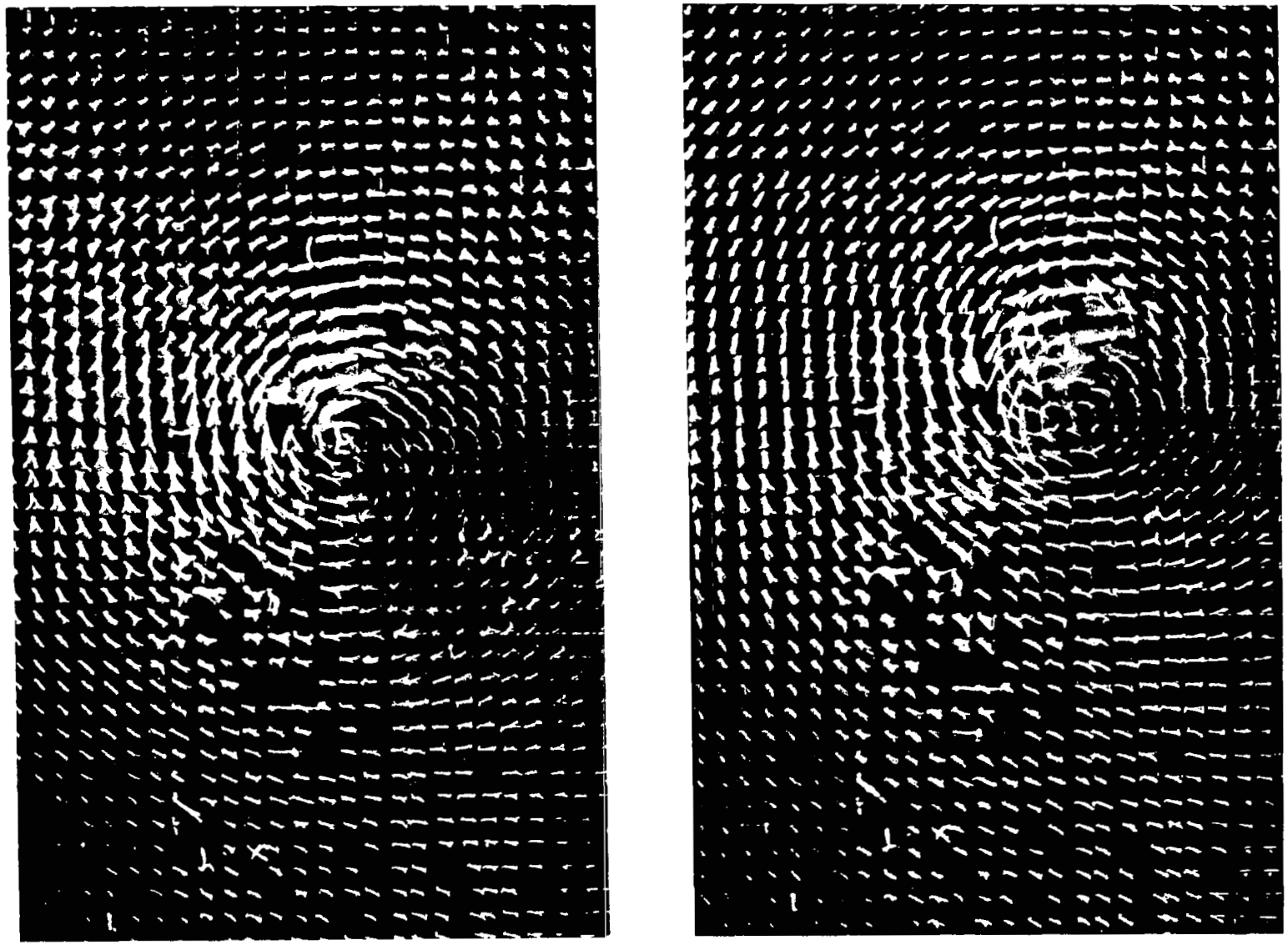

(b) 7 chord lengths downstream.

Figure 22.- Continued.

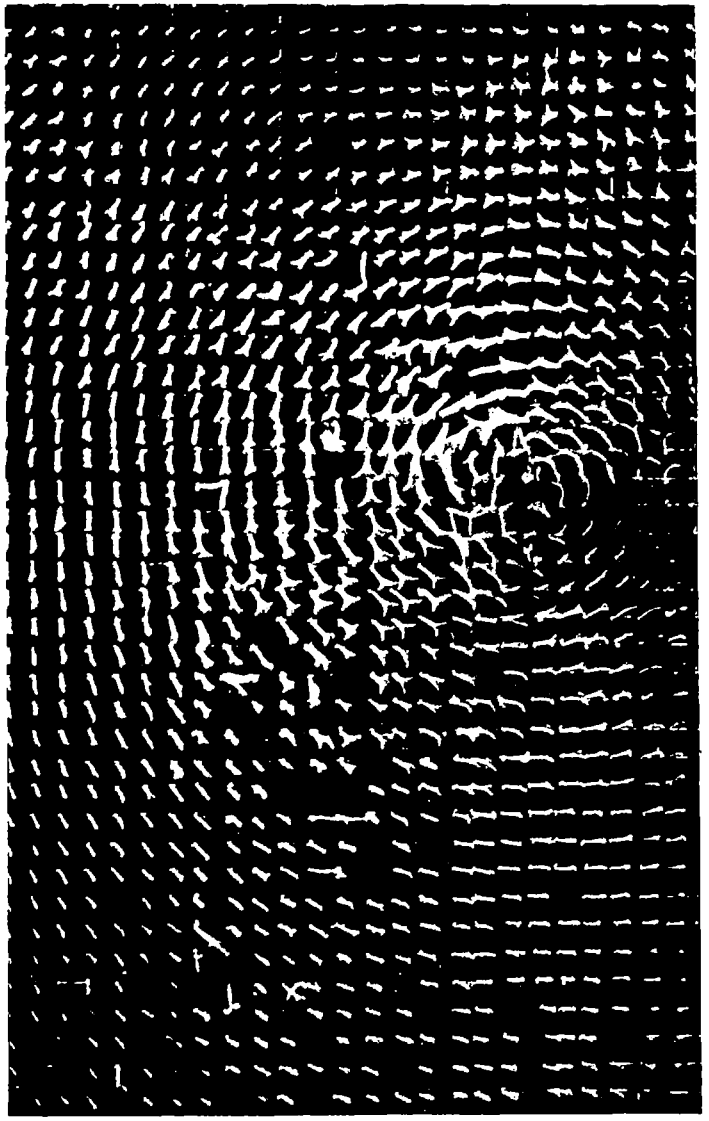

(b) Concluded.

Figure 22.- Concluded.

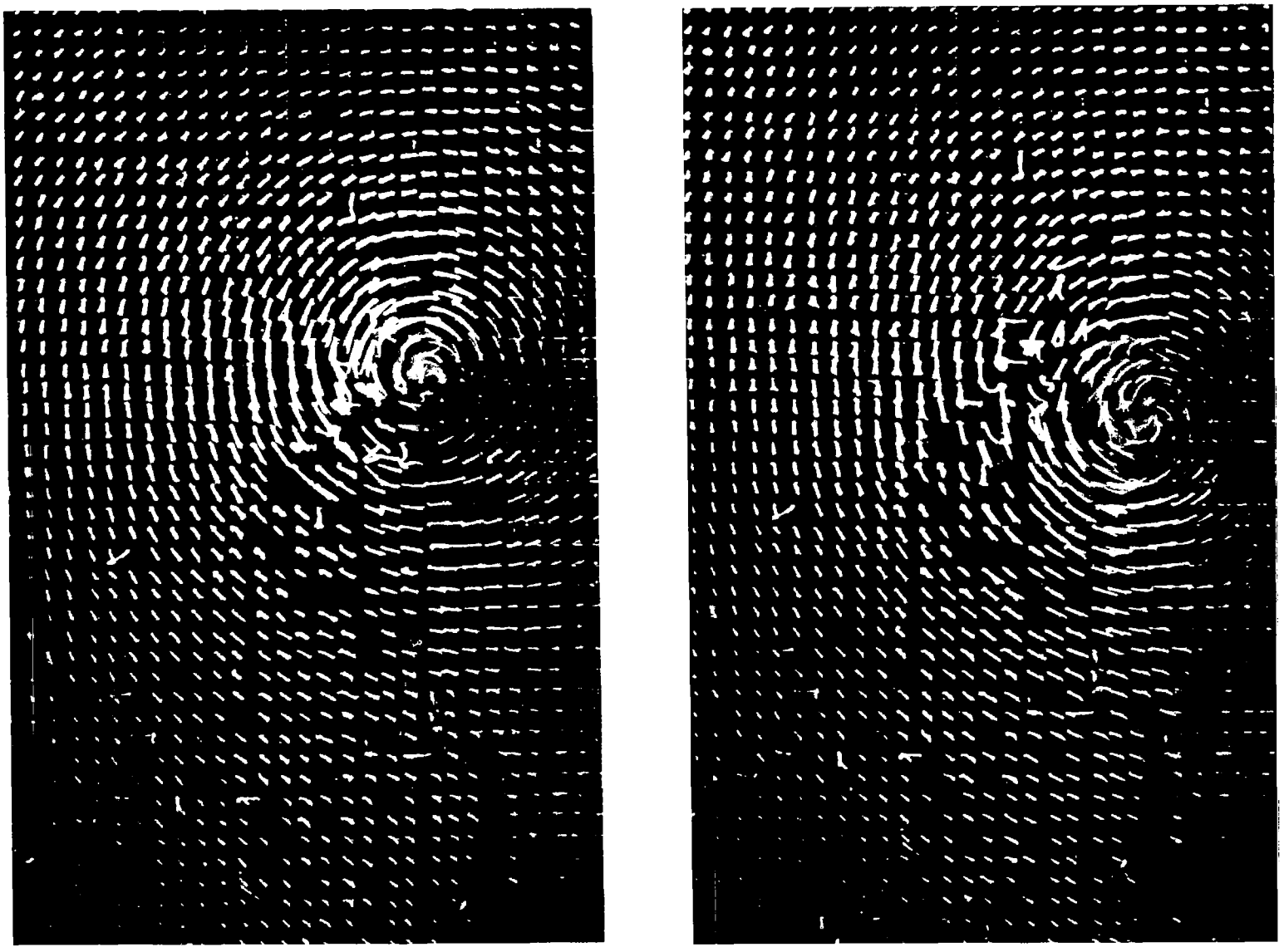

(a) 5 chord lengths downstream.

Figure 23.- Tip-vortex cross-sectional characteristics for configuration 5. $\alpha = 18^{o}$; 1-in. (2.54 cm) grid spacing.

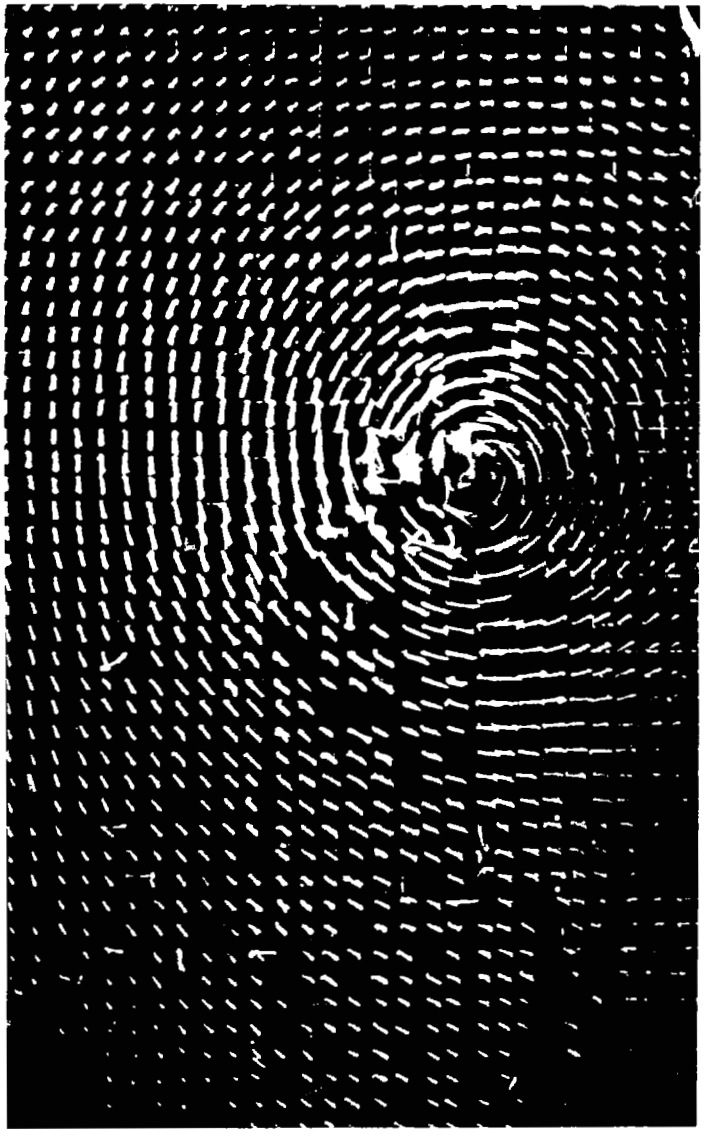

(a) Concluded.

Figure 23.- Continued.

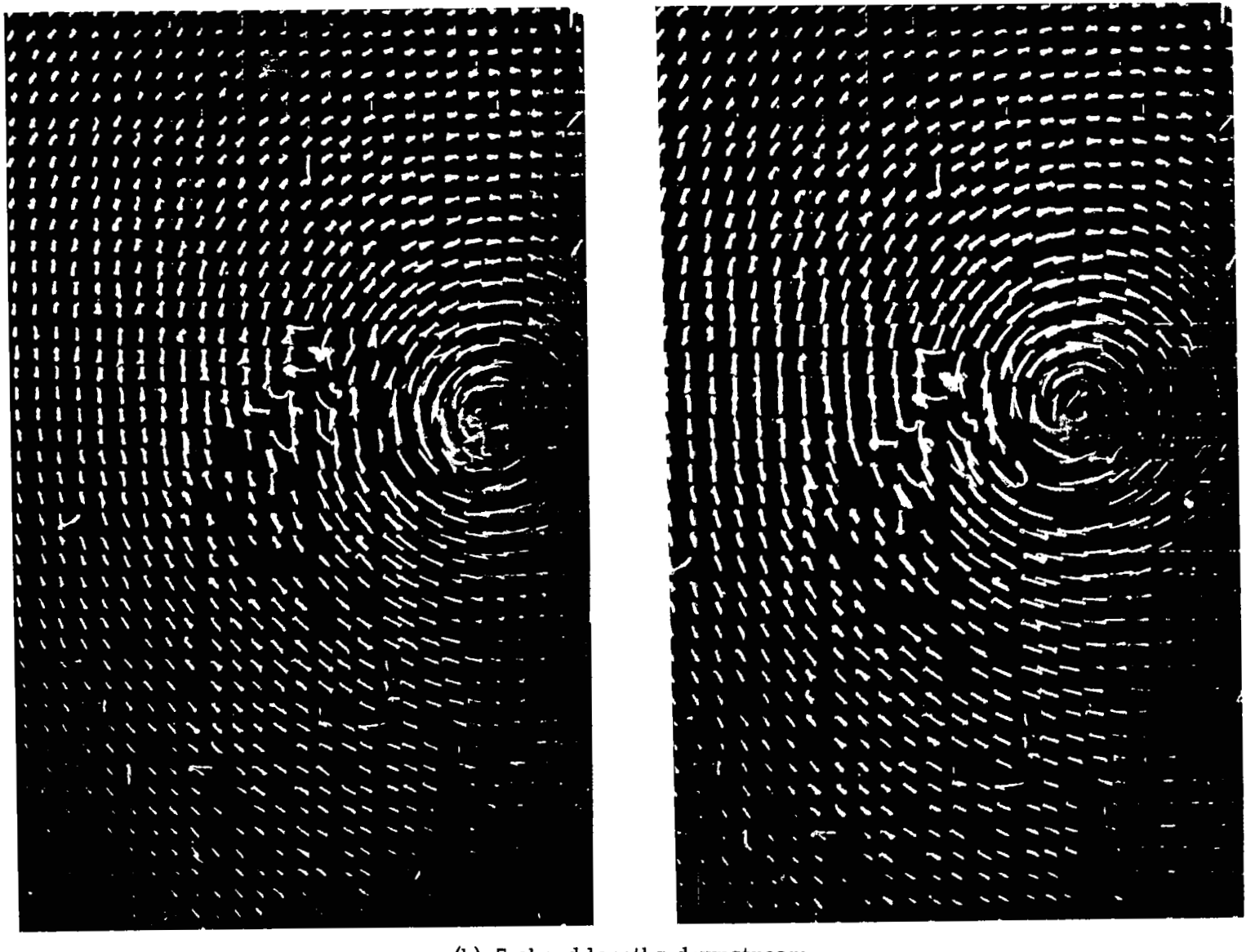

(b) 7 chord lengths downstream.

Figure 23.- Continued.

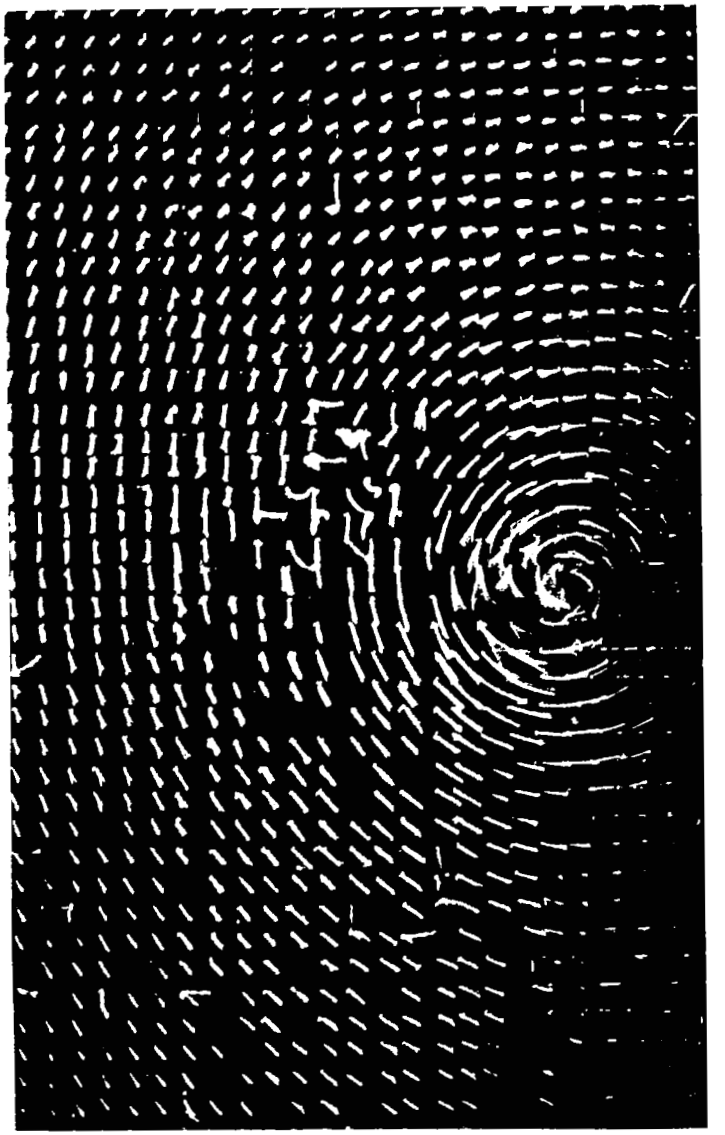

(b) Concluded.

Figure 23.- Concluded.

"The aeronautical and space activities of the United States shall be conducted so as to contribute . . . to the expansion of human knowledge of phenomena in the atmosphere and space. The Administration shall provide for the widest practicable and appropriate dissemination of information concerning its activities and the results thereof."

—NATIONAL AERONAUTICS AND SPACE ACT OF 1958

NASA SCIENTIFIC AND TECHNICAL PUBLICATIONS

TECHNICAL REPORTS: Scientific and technical information considered important, complete, and a lasting contribution to existing knowledge.

TECHNICAL NOTES: Information less broad in scope but nevertheless of importance as a contribution to existing knowledge.

TECHNICAL MEMORANDUMS: Information receiving limited distribution because of preliminary data, security classification, or other reasons.

CONTRACTOR REPORTS: Scientific and technical information generated under a NASA contract or grant and considered an important contribution to existing knowledge.

TECHNICAL TRANSLATIONS: Information published in a foreign language considered to merit NASA distribution in English.

SPECIAL PUBLICATIONS: Information derived from or of value to NASA activities. Publications include conference proceedings, monographs, data compilations, handbooks, sourcebooks, and special bibliographies.

TECHNOLOGY UTILIZATION PUBLICATIONS: Information on technology used by NASA that may be of particular interest in commercial and other non-aerospace applications. Publications include Tech Briefs, Technology Utilization Reports and Technology Surveys.

Details on the availability of these publications may be obtained from:

SCIENTIFIC AND TECHNICAL INFORMATION OFFICE

NATIONAL AERONAUTICS AND SPACE ADMINISTRATION

Washington, D.C. 20546